Design and Development of non-invasive RF-Based Prototype for Bone Health Evaluation

By

Ayesha Inam Tarar

(Registration No: 00000398861)

A thesis submitted to the National University of Sciences and Technology, Islamabad,

in partial fulfillment of the requirements for the degree of

Masters in

Computational Sciences and Engineering

Supervisor: Dr. Zartasha Mustansar

School of Interdisciplinary Engineering and Sciences

National University of Sciences and Technology (NUST)

Islamabad, Pakistan

January (2025)

THESIS ACCEPTANCE CERTIFICATE

Certified that final copy of MS/MPhil thesis written by Ms. <u>Ayesha Inam Tarar</u> Registration No. 00000398861 of __**SINES**__ has been vetted by undersigned, found complete in all aspects as per NUST Statutes/Regulations, is free of plagiarism, errors, and mistakes and is accepted as partial fulfillment for award of MS/MPhil degree. It is further certified that necessary amendments as pointed out by GEC members of the scholar have also been incorporated in the said thesis.
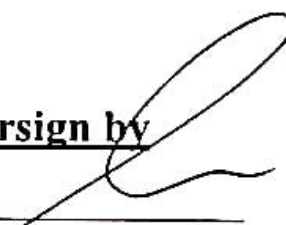
Signature with stamp: _____

Dr. Zartasha Mustansar
HoD SINES
Tenured Associate Professor
SINES - NUST, Sector H-12
Islamabad

Name of Supervisor: ___Dr. Zartasha Mustansar.___

Date: ___2-7- 1- 25___

Signature of HoD with stamp: _____

Dr. Mian Ilyas Ahmad
HcD Engineering
Professor
SINES - NUST, Sector H-12
Islamabad

Date: ___27/01/2025___

Countersign by

Signature (Dean/Principal): _____

Date: ___27/1/25___

AUTHOR'S DECLARATION

I <u>Ayesha Inam Tarar</u> hereby state that my MS thesis titled "<u>Design and</u>

<u>Development of non-invasive RF-Based prototype for Bone Health Evaluation</u>" is my

own work and has not been submitted previously by me for taking any degree from

National University of Sciences and Technology, Islamabad or anywhere else in the

country/ world.

At any time if my statement is found to be incorrect even after I graduate, the univer-

sity has the right to withdraw my MS degree.

Student Signature: _____

Name: Ayesha Inam Tarar

Date: 27 January 2025

PLAGIARISM UNDERTAKING

I solemnly declare that research work presented in the thesis titled "<u>Design and Development of non-invasive RF-Based prototype for Bone Health Evaluation</u>" is solely my research work with no significant contribution from any other person. Small contribution/ help wherever taken has been duly acknowledged and that complete thesis has been written by me.

I understand the zero tolerance policy of the HEC and National University of Sciences and Technology (NUST), Islamabad towards plagiarism. Therefore, I as an author of the above titled thesis declare that no portion of my thesis has been plagiarized and any material used as reference is properly referred/cited.

I undertake that if I am found guilty of any formal plagiarism in the above titled thesis even after award of MS degree, the University reserves the rights to withdraw/revoke my MS degree and that HEC and NUST, Islamabad has the right to publish my name on the HEC/University website on which names of students are placed who submitted plagiarized thesis.

Student Signature: _____

Name: Ayesha Inam Tarar

Date: 27 January 2025

DEDICATION

This thesis is dedicated to the people who have been my unwavering pillars of support throughout this journey.

- To my parents, whose unconditional love, sacrifices, and encouragement have been my foundation. Your belief in me, even during my most uncertain moments, has been my greatest strength. You have always inspired me to aim higher and never give up.

- To my mentor and supervisor, Dr Zartasha Mustansar, who guided me with her wisdom and patience. Her insights and feedback have shaped this work and taught me to think critically and to persevere through challenges.

- To my friends and all my Biomechanics lab mates, who have been my source of joy and relief, especially during moments of stress and doubt. Thank you for always reminding me to take a step back, laugh, and find balance.

ACKNOWLEDGEMENTS

Contents

List of Tables

List of Figures

VII

LIST OF SYMBOLS, ABBREVIATIONS AND ACRONYMS

- BMD Bone Mineral Density
- DEXA Dual Energy X-ray Absorptiometry
- RF Radio Frequency
- ISM Industrial, Scientific and Medical
- MICS Medical Implant Communication System
- CT Computer Tomography
- MRI Magnetic Resonance Imaging
- CST Computer Simulation Technology
- S-parameters Scattering Parameters
- SMA SubMiniature versionA
- PCB Printed Circuit Board
- DICOM Digital Imaging and Communication in Medicine
- ROI Region Of Interest
- CAD Computer Aided Design
- PLA Polyactic Acid
- VSWR Voltage Standing Wave Ratio
- VNA Vector Network Analyzer
- SAR Specific Absorption Rate

Abstract

Recognizing the growing prevalence of skeletal health disorders in developing countries, this study introduces a novel non-invasive radio frequency (RF)-based prototype for evaluating bone health. Conventional diagnostic methods, such as dual-energy X-ray absorptiometry (DEXA) scans, are hindered by factors such as limited accessibility, high costs, radiation exposure, necessitating the need of alternative, non invasive technologies. This research highlights RF technology to address bone health challenges by designing and optimizing a prototype that operates within the ISM frequency band. High-resolution CT scans were utilized to construct detailed 3D bone model, accurately capturing the anatomical complexities of cortical and trabecular layers. Two identical microstrip patch antennas were designed specifically for on-body operation at 2.45 GHz, ensuring performance tailored to this application.

A conceptual framework was developed, employing strategically placed antennas to analyze electromagnetic energy transfer through a bone model. Using both simulation and experimental methods, the study investigated the variations in transmission coefficients and scattering parameters (S-parameters). These parameters were used to assess the dielectric properties of the bone, which were assigned separately to the bone microstructure. Notably, trends in the s11 (reflection) and s21 (transmission) parameters were observed. Sensitivity tests based on dielectric properties and distance between antennas were also to check influence of energy interaction within the bone model. This study is unique in its content to offer deeper insights into the complex interplay between RF signals and natural structures, providing an essential foundation for the analysis of bone porosity and structural integrity.

Experimental findings demonstrated that the dielectric properties of the bone significantly influence the reflection and transmission characteristics of the antennas. Real-time measurements further validated these observations, highlighting the potential of this approach to provide insights into bone porosity and structure. This research highlights the transformative potential of RF technology in orthopedic diagnostics, offering a non-invasive, accessible, and safer alternative for bone health research. This method holds particular promise for regions where traditional diagnostic techniques are either unavailable or impractical. By pioneering this innovative solution, the study aims to contribute to global efforts in improving bone health management and reducing the burden of skeletal disorders.

Keywords: On-body matched antennas, Noninvasive assessment, ISM frequency band, Bone analysis, Early intervention

Chapter 1

Introduction

The rapid evolution of technology in healthcare, particularly with the integration of artificial intelligence, has made keeping pace with innovations a formidable challenge. Emerging advancements in mechanical, electrical and mechatronics engineering have revolutionized problem solving across healthcare domains, raising both opportunities and complexities.

Within biomedical engineering, biomechanics holds a distinct and critical position. This specialized discipline focuses on ths study of kinetics and kinematics of the skeletal system, offering insights into maintaining and improving bone health. Maintaining healthy bones is a lifelong pursuit, but it becomes even more crucial in developing nations like Pakistan. This, coupled with limited access to healthcare resources, including preventative measures and proper nutrition, can significantly compromise bone health. Bone health refers to the strength and integrity of bones, which is primarily determined by **Bone Mineral Density (BMD)** a quantitative measure of the concentration of minerals, predominantly calcium and phosphorus, within bone tissue. BMD serves a key indicator of bone strength and is typically measured using techniques like **Dual-Energy X-ray Absorptiometry (DEXA)**

Optimal bone health is characterized by a balance between bone resorption and bone formation, ensuring sufficient mineralization to withstand mechanical loads and resist fractures. A decline in BMD is associated with conditions like **osteopenia** and **osteoporosis**, increasing the risk of fractures and structural deformities.

Thus, BMD is not only a clinical marker for diagnosing bone related disorders but also a critical parameter for evaluating the efficiency of methods and techniques aimed at improving or maintaining bone health.

These factors contribute to conditions like bone demineralization, a loss of bone min-

erals that weakens bones, and osteonecrosis, a condition characterized by the death of bone tissue due to inadequate blood supply [3]. Left unchecked, these issues later, can progress to osteoporosis, a widespread skeletal disorder affecting over 200 million people globally [4]. Osteoporosis is characterized by reduced bone density and increased susceptibility to fractures, particularly in critical areas like the hip, spine, and wrist. These fractures can be debilitating, causing immense pain, *loss of mobility*, and even increased mortality rates. The societal and economic burden of osteoporosis is significant. Fractures often lead to hospitalization, long-term care needs, and lost productivity, placing a strain on healthcare systems and economies worldwide. Furthermore, a precursor to osteoporosis called osteopenia often goes undetected due to its asymptomatic nature [5]. Individuals with osteopenia may not experience any symptoms until a fracture occurs, highlighting the importance of early detection and preventative measures for maintaining bone health throughout life. Beyond age and gender, several other factors contribute to bone health decline. Inadequate intake of calcium and vitamin D, essential nutrients for bone growth and maintenance, are major risk factors. Lack of physical activity, smoking, excessive alcohol consumption, and certain medications can also weaken bones and increase the risk of osteoporosis.

Traditional methods for bone health assessment, such as Dual-Energy X-ray Absorptiometry (DEXA) scans, have limitations. DEXA scans utilize two different X-ray energy levels to measure bone mineral density (BMD), a key indicator of bone strength. By comparing the absorption rates of these X-ray beams by bone and soft tissue, DEXA scans can estimate the amount of minerals present in the bones being scanned. While DEXA scans are a widely used and relatively affordable diagnostic tool for osteoporosis, they have several drawbacks. One major concern with DEXA scans is their use of ionizing radiation. While the radiation dose associated with a single DEXA scan is relatively low, frequent monitoring can lead to cumulative exposure, raising concerns for some patients. Additionally, DEXA scans may not be suitable for everyone, such as pregnant women or individuals with certain medical implants. Another limitation of DEXA scans is their inability to distinguish between different bone types. Bone is composed of two main types: cortical bone, which is dense and strong, and trabecular bone, which is more porous and lightweight. DEXA scans provide a **single BMD value** that represents an average for the scanned area, potentially masking underlying issues. For instance, a patient with primarily deteriorating trabecular bone may have a normal DEXA scan result despite being at an increased risk of fracture. These limitations of DEXA scans highlight the need for alternative bone health assessment techniques that are safe, accurate, and can provide a more detailed picture of bone health.

This study therefore explores the potential of Radio Frequency (RF) technology as a non-invasive and potentially more comprehensive approach to bone characterization

analysis. RF technology refers to the utilization of electromagnetic waves within a specific frequency range, typically from around 3 kHz to 300 GHz. These waves consist of oscillating electric and magnetic fields that can travel through space or various mediums, including air, tissues, and even bone. The interaction of RF waves with matter depends on the material's properties, such as its electrical conductivity and permittivity (ability to store electrical energy). When RF waves encounter bone tissue, some of the wave's energy is absorbed by the bone, while the remaining portion transmits through it. By analyzing the characteristics of the transmitted and absorbed waves, information can be gathered about the bone's composition and health. RF technology has a wide range of applications such as in the field of Wireless Communication, including Wi-Fi, Bluetooth and in Radio frequency Identification (RFID) tags to store and transmit data about objects, for tracking, and managing access control systems. Some of the examples of RF technology in the medical field beyond bone health assessment [6]

1. Radiofrequency ablation (RFA): This technique utilizes RF waves to generate heat and destroy targeted tissue, commonly used in cancer treatment and pain management.

2. Magnetic resonance imaging (MRI): Although not directly using RF waves itself, MRI scanners employ strong magnetic fields and pulsed RF signals to create detailed images of internal organs and tissues.

3. Diathermy: This therapy uses RF waves to generate deep heat within tissues for therapeutic purposes, such as pain relief and promoting tissue healing.

The potential benefits of RF technology for bone health assessment lie in its non-invasive nature and its ability to interact with bone tissue. By analyzing the interaction of RF waves with bone, researchers hope to gain insights into various bone health parameters, including: Bone mineral density (BMD).

The strength of this study is based on the potential of RF technology to estimate BMD using fine bone microstructure of a living vertebrate by analyzing the absorption and transmission of RF waves. The porous structure of bone can be assessed by analyzing how RF waves interact with the different level of details in the bone, including the solid mineralized matrix and air-filled spaces. Many studies rely on simplified bone models that may not fully capture the complexities of real bones, such as the intricate structures of the femur [7, 8]. However, existing research on RF-based bone health monitoring offers promise but has limitations. These limitations hinder the development of accurate and reliable RF-based diagnostic tools. Additionally, research also catered antenna design optimization and placement for efficient signal interaction with bone tissue while ensuring user safety.

1.1 Research Gap

This research integrates RF technology to address the critical gap in traditional methods such as, DEXA scans and explore its applications in orthopedic engineering. The study focuses on using RF-technology to assess bone health based on real bone microstructures, aiming to develop a safe, non-invasive, and portable technology as an alternative to the hardcore DEXA setup.

1.2 Aims and Objectives

This research aims to develop an innovative RF-based bone health monitoring system that addresses the limitations of existing methods. The specific objectives are:

1. **Device Design and Development:** Design and develop a prototype of strategically placed on body-matched antennas for efficient signal transmission through the human body. Deploy an anatomically realistic 3D bone model from CT scans, replicating the dielectric properties of the actual femur bone using secondary data. The recommended model will incorporate intricate microstructure details, unlike simplified models used in the previous research. Afterwards, designing the system which allows individuals to easily monitor their bone porosity and bone health based on bone mineral density (BMD).

2. **RF technology in Orthopedics:** Integrate RF technology with a low operating frequency within the allowable ISM band to prioritize user safety by ensuring a non-invasive and radiation-free technique.

3. **Smart & Feasible Monitoring:** Developing a portable device for easy monitoring of bone porosity and bone health based on bone mineral density (BMD). This will enable continuous, long-term monitoring of bone health, facilitating early detection of bone loss and enabling preventative measures to reduce fracture risk.

Impact of research: This research emphasizes the innovative potential of RF technology for bone health evaluation by utilizing its capacity to estimate bone mineral desity (BMD) through interactions with detailed bone microstructures. By overcoming current limitations in RF-based diagnostic methods and refining antenna design for improved signal precision and user safety, this study provides a foundation for developing non invasive, real-time tools for monitoring bone health. These advancements could significantly enhance early diagnosis and management of bone-related conditions, addressing the complexity of living bone architecture with greater scientific accuracy.

1.3   Thesis Outline

Every section and chapter of this thesis has been developed on the optimum detail to provide an extensive approach toward designing a prototype for bone health evaluation for early detection and prevention of bone diseases like Osteopenia. The proposition is divided into numerous highly relevant segments, which focus on separate aspects of the research methodology and the outcomes.

The previously described **Introduction** section bring into effect again the study context and establishes the research motives based on the necessity of preventing bone diseases, minimizing the risk of fractures and injuries among elder women especially. The following section avails the reader of a clear understanding of what is being discussed, as well as the motivation for conducting the research.

The second chapter is **Literature Review** analyses for microstrip patch antenna design and development for medical applications, such as bone health detection. Thus, the given text covers the current state of injury prevention using RF technology for bone health assessment, traditional solutions, and the notion of biomimetic bone design for evaluation. This review defines the gaps in knowledge that can be discerned from the past literature, which forms the premise for the novel approaches explored in this thesis.

The third chapter is **Methodology** section explains the means used to design the antenna to assess the effectiveness of RF technology for bone health evaluation. The text tells the flow of how 3D bone model has been developed with the help of CT scans, and the development of experimental set up for hardware simulations. It is the section that also explains the software and hardware testing processes for two antennas with and without the bone model placed in the middle.

The second last chapter **Results and Discussion** section on the other hand gives detailed view of the findings gotten from, the software and hardware simulations. To assess the performance of antennas with, real animal bone model for the hardware simulations and anatomically realistic 3D bone model for software simulations. We compare the S11 and S21 parameters of antennas against each simulation, of varying the distance with the bone model. Such outcomes are discussed in the context of advantages of RF technology in evaluating the bone health and preventing the risk of injury.

The last chapter of the thesis is entitled **Conclusion and Future Work** in which the leads to the major findings of the thesis, the research contributions to development of a prototype for non-invasive antenna design for bone health evaluation and mitigation of risk of injuries, and the outline of the foreseeable future research in field are given.

Chapter 2

Literature Review

The structure of this thesis is designed to reflect the progressive stages of this research, aligning with the objectives as guided storyboard to develop a more accurate, non-invasive and a non-ionizing method for bone health assessment using RF technology. Initially, the research analyzes the invasive and ionizing current RF technology methods for bone health evaluation. This foundational analysis is crucial for understanding the scope of the study. Moving forward, research investigates into the critical stage of simulation and experiments, examining the various bone models used in previous studies. The literature review, methodology, and results of each of these parts enable a more thorough comprehension of the individual contributions to the overall objective and results.

2.1   Integration of RF Technology in Health-care

Radio Frequency (RF) technology is a widely adopted technology in healthcare due to its versatility. This technology uses the electromagnetic (EM) waves, and typically range between (3Khz to 300 GHz). It can penetrate human body as implantable sensors, and non-invasively which makes it suitable for diagnosis and monitoring.

The integration of RF-based devices with the use of Electromagnetic (EM) waves sensors are emerging as a revolutionized tool in healthcare, by offering innovative and cost-effective approaches. RF technology can be applied to human body for sensing, monitoring, and diagnosis purposes, a wide range of applications include: implantable devices, wearable devices to be worn on the body, to monitor vital signs, detect diseases, and track patient activity as represented in Figure 2.1 . There are Implantable antennas and sensors designed to continuously monitor glucose levels, to track bone healing progress, and even for brain activities, enabling real-time insights into a patient's well being. Wearable devices, such as smartwatches exist for personalized health management, providing continuous monitoring of heart rate, blood oxygen and glucose

levels. Additionally, these sensors are accustomed to remotely monitor elderly individuals and patients in case of emergencies. Furthermore, electromagnetic sensors find applications in bio sensing, radar-based sensors. RF technology has vast applications in healthcare and these sensors hold immense potential for improving patient care, enabling early disease detection. [1, 9, 10]

Figure 2.1: Applications of RF Technology using Electromagnetic (EM) waves in healthcare[1]

2.2 Applications of RF-Based Implantable Devices in Healthcare

To date, one of the vital components of implantable devices (IMDs) are antennas, used as the source of signal reception and transmission. Over a period of time these implantable antennas have been widely used in numerous applications including body-monitoring, disease diagnosis, and bio-telemetry [1]. In this section, we will discuss scenarios, how implantable antennas have been used in healthcare and patient monitoring.

8

Glucose monitoring: Today, diabetes is considered as, one of the most serious chronic and prevalent disease, it has affected over 537 million individuals. Death toll due to diabetes has crossed a figure of over 6.7 million as reported by The International Diabetes Federation (IDF) in 2021, these numbers are increasing significantly [11]. For monitoring the levels of blood sugar, in human body, continuously implantable devices have been used. In [12], Implantable antennas operating in dual-band frequency, MICS (402 MHz) and ISM (2.45 GHz), was considered to be an efficient way to save energy between the two modes of the patient; sleep and waking-up. In [13], A Silicon Carbide (SiC) biocompatible material sensor was used for monitoring blood glucose continuously. It used radio frequency (RF) signals for the monitoring purpose and the shift in resonance frequency of the sensor indicates the changing levels of blood glucose, if frequency ranges between 40MHz and 26MHz, then the change in blood glucose levels ranges from 120 mg/dl to 530 mg/dl respectively. In [14], Implantable, compact in size antenna operating within ISM band (2.40–2.48 GHz) was designed and experimented as a real-time glucose monitoring application of implantable antennas.

Brain Disease Diagnosis: Implantable antennas, are widely considered for detection of brain related diseases, for monitoring and early detection in case of anomalies, such as tumor cells. Wireless brain implants were designed, keeping in mind the convenience of the patients, as wired devices may cause impairment or restrict their mobility. In [15], miniature implantable antenna with an operating frequency in MICS band (402–405 MHz), is projected as a portion recording device for brain-machine interference (BMI). It was for the first time, where authors were investigating consequences of thermal noise in biomedical by means of absorption analysis.

Bone Health Analysis: Traditional imaging techniques like MRI, X-rays, and CT scans are commonly used for bone health analysis, but have limitations: they are costly, not easily accessible and ionizing. Researchers have discovered invasive or implantable antennas as a valuable tool for assessing bone healing, the analysis is based on variations in electromagnetic (EM) waves. Implantable antennas for bone health analysis include applications such as, monitoring the bone healing progress after a surgery is critical, as recovery time varies for each patient. Multiple factors like age, nutrition, and underlying health conditions may cause delayed healing, which can then lead to persistent pain and weakens the muscles. In [16], an antenna was proposed for managing bone fracture recovery, as a part of fixation metal plates. Implanted antenna embedded; Echidna Pin helps in accurate monitoring, and to assess healing progress through signal processing. Another study [17] presented monopole antennas using RF technology for external support to fractured bones with fixation screws. By tracking power transfer between these antennas, fracture healing progression can be evaluated. Further provided insights into bone healing progress using dual monopole antennas. Authors in [7] proposed two different antennas; planar and meander half-wave dipole antenna operating within the range of 100 MHz to 10 GHz. This study approves that the propagation of electromagnetic (EM) wave through a multi-layered human tissue

can be used to differentiate between a normal and fractured bone, by measuring the differences in power densities transmitted over an average. Experimental validation was performed on animal models to propose the feasibility of this method as a non-invasive and efficient solution for continuous healthcare monitoring of bone fractures. Main focus of our research is evaluate the bone health of patients using the RF technology. Over the years, implantable antennas have been thoroughly discussed and been utilized increasingly to address bone health monitoring challenges by enabling continuous and precise monitoring. In this review, we will discuss how various researchers have employed implantable antenna systems, highlighting their antenna designs, operating frequencies, and applications for bone health evaluation.

2.3 Implantable RF based technologies for Bone Health Evaluation

Implantable RF technologies have emerged as groundbreaking solutions for monitoring and diagnosing bone health. By utilizing advanced antenna designs, these systems enable precise and efficient communication within the human body, offering real-time data on bone conditions such as fractures, healing progress, and even osteoporosis. In [18] a microstrip patch antenna tailored for healthcare monitoring applications was developed, specifically operating within the 2.45 GHz ISM band. With a size of 4×5.5×0.254 mm^3, the antenna demonstrated excellent return loss (47 dB) and sufficient bandwidth (20 MHz) to enable accurate signal transmission for monitoring bone mineral density (BMD) and general bone health. Its compact form and low power requirements align well with stringent safety standards, making it an effective implantable device for long-term bone health tracking.

In the context of bone fracture recovery, [17] proposed a monopole antenna system implanted into the fracture site. These antennas, embedded in stabilization hardware like screws or external fixators, monitored healing by analyzing RF signal variations across the fractured bone. As the fracture healed, the transmitted power reduced, correlating with the diminishing hematoma volume. This technique provided doctors with quantitative feedback on the progress of healing in bones such as the radius, tibia, and phalanges, as validated through both phantom and ex-vivo lamb femur experiments.

Implantable antennas, while offering direct interaction with the target tissue, present several significant challenges and limitations for bone health evaluation. The invasive nature of these devices inherently involves surgical procedures, which carry risks such as infections, complications, and discomfort for the patient. Additionally, implantable systems often require biocompatible materials and energy-efficient designs to minimize tissue irritation and extend the device's operational lifespan, adding complexity and

cost to the development process. Long-term monitoring using implantable antennas can also raise concerns about device stability, as bodily movements, bone remodeling, or inflammatory responses may alter the antenna's positioning or performance. Moreover, the practicality of widespread deployment is limited by the need for specialized surgical skills and post-operative care, making these devices less suitable for routine or large-scale bone health monitoring

In contrast, non-invasive RF technology eliminates these complications by utilizing externally applied antennas to evaluate bone health. This approach has been critically reviewed in the following subsection.

2.4 Non-invasive RF based technologies for Bone Health Evaluation

RF technology leverages the interaction of electromagnetic waves with biological tissues to provide insights into bone structure and composition without ionizing radiation. This section critically analyzes the advancements in this field by examining the methodologies, antenna designs, operating frequencies, and applications of RF-based systems as presented in the literature.

[19] developed a circularly polarized antenna operating in the 2.25–2.78 GHz range for real-time bone health monitoring. The antenna, designed with L-shaped slots to enhance impedance matching and bandwidth, was compact (42 × 1.27 mm*), enabling its application in microsystems. Simulated tissue environments were used to validate the system, replicating the dielectric properties of cortical and trabecular bone layers. While the study demonstrated the antenna's potential for monitoring osteoporosis-related changes, the exclusive reliance on simulations posed limitations for clinical translation. The antenna was tested at a negligible distance from the bone model to mimic a real-world application scenario, ensuring direct interaction with simulated tissues.

[20] presented a folded dipole RFID tag antenna for continuous osteoporosis management. Operating in the 2.4–2.48 GHz ISM band, this antenna measured 10 × 15 × 2 mm* and was validated using a human arm phantom. The system demonstrated the capability to monitor bone density changes by analyzing variations in dielectric properties over time. The experimental setup ensured close proximity to the body, with the antenna placed subdermally on the phantom, allowing accurate data capture. However, despite its non-invasive design, the system exhibited limited gain (-16.3 dBi), necessitating further optimization to enhance signal transmission and reliability in diverse real-world conditions.

[21] investigated ultra-wideband (UWB) antennas for wireless bone health evaluation. Their antennas, capable of operating across a wide frequency range, were applied

in fracture assessment, neural monitoring, and bone density analysis. The experimental setup involved tissue-mimicking phantoms and in-vivo tests to analyze signal propagation and path loss. The antennas were positioned on the skin surface for on-body applications, ensuring minimal separation from the target site. The broad bandwidth facilitated the detection of subtle dielectric property changes, although challenges such as variable tissue composition and path loss required further refinement to ensure consistent performance across different anatomical sites.

[22] developed a wearable RF-based microstrip patch antenna initially designed for hydration monitoring but later adapted for bone health diagnostics. Operating at 2.4 GHz, the antenna analyzed reflected and transmitted signals to detect changes in dielectric properties associated with bone porosity and density. The experimental setup involved simulations and human trials, with the antenna placed directly on the skin to ensure accurate interaction with underlying tissues. While the study demonstrated the potential of wearable RF systems, environmental factors like temperature and humidity were identified as sources of interference, requiring calibration for precise diagnostics.

[23] explored a novel integration of RF signals with photoacoustic temporal profile analysis to assess bone mineral density. The system used RF energy to generate photoacoustic waves, which were analyzed to infer bone porosity. The methodology primarily relied on simulations, highlighting strong correlations between dielectric properties and density changes. While this approach demonstrated significant potential for enhancing diagnostic accuracy, the absence of experimental validation using real bone samples limited its clinical applicability. The system's design emphasized direct interaction with the target tissue, ensuring minimal separation for optimal signal capture.

[24] employed acoustic RF signals to monitor bone healing and differentiate between healthy and osteoporotic bones. Their system operated at acoustic resonant frequencies and demonstrated sensitivity to structural variations in bone porosity and density. Simulations and controlled experiments on phantoms were conducted, with the antenna placed in close proximity to the bone model. The reliance on simplified models, however, posed challenges for replicating in-vivo conditions and necessitated further validation with realistic anatomical setups.

[25] utilized photothermal radiometry integrated with RF technology to detect osteoporotic bone loss. The study focused on non-invasive thermal analysis, using RF-induced modulated luminescence to measure changes in bone properties. Tissue-mimicking phantoms were used to validate the system, with the antenna positioned directly on the skin to optimize signal interaction. While the study highlighted the sensitivity of RF systems in detecting early-stage osteoporosis, the dependency on controlled conditions limited its practicality for broader diagnostic applications. Critically analyzing these studies reveals several trends and gaps. Most RF-based approaches rely on microstrip patch antennas operating near the ISM frequency band of 2.4–2.5 GHz, favored for their compactness and compatibility with biological tissues. Applications range from monitoring bone healing to detecting osteoporosis and evaluating

bone porosity. However, many studies use simplified models, such as drilled bovine bones or phantoms, which fail to capture the complexities of human bone structures. Furthermore, while simulation results often show high accuracy, experimental setups frequently face challenges in achieving the same level of precision due to variations in dielectric properties and environmental factors. A rectangular microstrip patch antenna, operating at 2.44 GHz with a fiberglass substrate (ε_r = 4.4) and dimensions 37.4 × 29.2 mm, is specifically designed for measuring bone mineral density (BMD), diagnosing osteoporosis, and classifying bone samples using machine learning algorithms. By evaluating silica, bone powder, and bovine femur samples at a 12 cm distance, simulations confirm its effectiveness in identifying bone density variations and distinguishing between healthy and osteoporotic states.

The circular microstrip patch antenna in [26], with a frequency range of 2.4–2.48 GHz, employs an FR4 substrate (ε_r = 4.3) and dimensions of 42.46 × 48.46 mm. It is primarily utilized for detecting breast cancer via breast phantoms modeled using CST simulations, effectively observing tumor-related changes in radiation parameters and directivity. Despite its robust simulation results, the absence of a defined source-to-sample distance poses limitations in clinical reproducibility.Moreover the stubbed planar monopole antenna, covering the ultra-wideband (UWB) range of 3–7 GHz, features a Rogers 5880 LZ substrate (ε_r = 1.98) and dimensions of 30 × 40 × 1.016 mm. Its primary application is in osteoporosis diagnosis and fracture prevention, using a human wrist phantom tested at multiple distances (4 mm to 18 mm). Temporal and frequency domain analyses validate its ability to detect early bone health anomalies, making it suitable for dynamic bone condition monitoring.

The dual dipole patch antenna in [27], operating within the 860–960 MHz range on a PET substrate, is a larger design (110 × 150 mm) focused on fracture monitoring through s-parameter variations. It uses cylindrical arm phantoms for low-cost, non-invasive monitoring, presenting a promising solution for regular health assessments.

Finally, the Christmas snowflake monopole antenna in [28], with a wide frequency range (4.9–12.6 GHz) and a cotton substrate (ε_r = 1.8), offers wearable functionality for non-invasive osteoporosis detection. Tested on cylindrical wrist models, this compact antenna (41.9 × 29.2 mm) integrates machine learning to enhance diagnostic accuracy, particularly for on-the-go health monitoring.

These advancements align with emerging trends in RF-based diagnostics, as demonstrated in studies like [29], who used a bow-tie antenna and clustering techniques for osteoporosis detection, and [30], who developed on-body antenna arrays for wrist bone signature measurements. These studies, along with hydrogel-based RFID sensing [31] and adaptive RF powering systems [32], reinforce the role of RF systems in non-invasive and wearable health monitoring technologies. These findings collectively underscore the transformative potential of RF-based systems in revolutionizing bone health monitoring by integrating cost-effective, non-ionizing, and wearable designs with advanced diagnostic capabilities.

This detailed analysis of existing literature contextualizes your work within the broader field of RF-based bone health evaluation, highlighting its contributions to addressing key limitations in current methodologies.

2.5 Antenna Design for RF Applications

Antenna design plays a pivotal role in the development of non-invasive RF-based technologies for bone health evaluation. Various studies have explored the design, optimization, and performance of antennas, focusing on their ability to interact with biological tissues and deliver reliable diagnostic results. This section critically examines the principles of microstrip patch antennas, their design challenges, and key performance metrics, incorporating findings from recent studies to evaluate their suitability for biomedical applications.

Microstrip Patch Antennas for Biomedical Applications Microstrip patch antennas are widely regarded as suitable for biomedical applications due to their compact size, ease of fabrication, and ability to operate efficiently within the ISM band (2.4–2.5 GHz). A study [33] presented a dual-band microstrip antenna designed for on-body operation. This antenna utilized a low-loss Rogers RT5880 substrate to enhance impedance matching and ensure efficient operation near biological tissues. The results demonstrated a reflection coefficient (s11) of less than -10 dB at 2.4 GHz, indicating minimal energy loss during signal transmission. The study further highlighted the importance of substrate selection in minimizing dielectric loss caused by proximity to biological tissues.

Similarly, [34] developed a rectangular microstrip patch antenna specifically for bone health monitoring. The antenna's compact design allowed for placement on the skin surface, ensuring optimal signal penetration into underlying bone tissues. Operating at 2.45 GHz, the antenna exhibited a gain of 5.2 dBi and a bandwidth of 30 MHz. The dielectric properties of bone were incorporated into the simulations, revealing significant variations in s21 transmission coefficients corresponding to different bone porosity levels. These findings underscored the antenna's sensitivity to structural changes in bone tissue.

Design Challenges in Antenna Development Despite their advantages, microstrip patch antennas face challenges in miniaturization, impedance matching, and maintaining performance when used on-body.[35] emphasized that the proximity of antennas to biological tissues introduces additional dielectric losses, which can degrade performance. To address this, the study employed a stacked patch design and integrated electromagnetic bandgap (EBG) structures to improve efficiency. The optimized antenna achieved a reflection coefficient of -18 dB at 2.45 GHz and a gain of 6 dBi, outperforming conventional designs in terms of on-body performance.

The challenge of impedance matching was also critically analyzed in [36], who inves-

tigated the impact of different substrate materials on antenna performance. Using substrates with varying dielectric constants, the study found that high-dielectric substrates reduced antenna size but adversely affected bandwidth and gain. The authors proposed a trade-off between compactness and efficiency, highlighting the need for tailored designs based on specific biomedical applications.

Antenna Performance Metrics, key metrics such as s11, bandwidth, and gain are critical for evaluating the performance of antennas in biomedical applications.[37] analyzed the impact of varying dielectric properties on these metrics. Their study revealed that the dielectric properties of bone significantly influenced signal reflection and transmission, with denser cortical bone exhibiting lower s21 values compared to porous trabecular bone. The study used a microstrip patch antenna with a rectangular slot to improve bandwidth, achieving a 50 MHz range at 2.4 GHz. These enhancements were critical for capturing the subtle variations in dielectric properties associated with bone health.

The reviewed studies consistently demonstrate the importance of substrate selection, antenna geometry, and impedance matching in achieving high performance in non-invasive bone health evaluation. However, many rely on simplified models or homogeneous tissue environments, which fail to account for the complexities of real bone structures. By incorporating anatomically realistic bone models and advanced antenna designs, future research can bridge this gap and enhance the reliability of RF-based diagnostics.

2.6 Bone Models for experiment and simulations

The use of non-invasive RF technology for bone health evaluation often necessitates the development of realistic models to simulate bone tissue's electromagnetic properties. In many studies discussed earlier, such as those involving RF antennas for monitoring bone porosity or density, phantoms were employed as surrogate models for human or animal bones, as shown in Figure 2.2. These phantoms, whether predefined, software-based, or derived from natural materials, serve as a critical intermediary to validate the accuracy and reliability of RF systems. This section explores the diverse types of phantoms used in RF applications, their development methods, and their roles in advancing bone health diagnostics.

Predefined Phantom Models in Literature Predefined phantoms are frequently utilized in RF studies to emulate the dielectric properties of bone and surrounding tissues. [21] used tissue-mimicking phantoms to test ultra-wideband antennas for bone density analysis. The phantoms were composed of hydrogel-based materials, which replicated the dielectric properties of cortical and trabecular bone. These phantoms were integral to evaluating signal propagation and attenuation, ensuring the antenna's performance in realistic conditions. Similarly,[20] employed a human arm phantom for
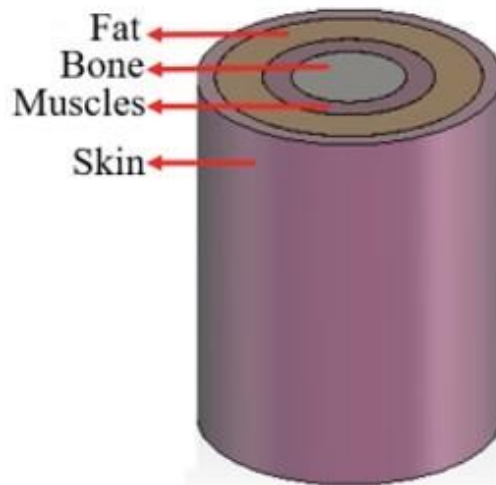
Figure 2.2: Multilayer homogeneous layer illustration containing Bone, Muscle, Fat and Skin of Human Wrist [2]

their RFID antenna experiments. The arm phantom mimicked subcutaneous tissues and bone structures, allowing precise validation of dielectric property measurements associated with osteoporosis progression.

Custom Phantoms Using Soil and Natural Materials Some researchers have explored innovative methods to create phantoms using natural materials. [19] highlighted the use of soil-mimicking materials to replicate the conductivity and permittivity of bones. By blending clay and organic matter, researchers developed phantoms that captured the dielectric variations of trabecular structures. This approach offered a low-cost alternative to synthetic phantoms while maintaining sufficient accuracy for RF testing. The resulting models were used to assess the interaction of circularly polarized antennas with varying bone densities, emphasizing the potential of such phantoms for real-world diagnostic applications.

Software-Defined Phantoms Software simulations play a pivotal role in developing phantoms for RF analysis.[23] utilized computationally generated phantoms to replicate bone mineral density changes. These phantoms were based on high-resolution CT scan data, allowing precise modeling of cortical and trabecular layers. By integrating these software-defined models with photoacoustic RF systems, researchers achieved detailed temporal profiles of bone density. While software phantoms provide unmatched control over structural parameters, their lack of physical validation highlights the importance of coupling these methods with experimental setups.

Bovine Bone Models The use of bovine bones as natural phantoms has also gained traction in RF research. In [24], authors conducted experiments on bovine bones to monitor healing and detect osteoporosis. Bovine bones, being structurally similar to human bones, provided an ideal platform to study the effects of dielectric property

changes on RF signal reflection and transmission. These experiments demonstrated the sensitivity of acoustic RF signals to bone porosity variations. However, the limitations of bovine models include their homogeneity compared to human bones and the inability to represent complex geometries.

[3] employed bovine bone samples to evaluate the effectiveness of microstrip antennas in characterizing bone tissue. The study aimed to analyze the interaction of electromagnetic waves with bone to detect structural changes and variations in dielectric properties. The microstrip antennas were designed to operate within the microwave frequency range, optimizing their sensitivity to the dielectric properties of bone tissue. These antennas provided accurate measurements of bone conductivity and permittivity, offering a foundational understanding of how electromagnetic signals interact with bone.

The experimental setup placed the bovine bone samples in a controlled environment to ensure consistency in signal propagation and minimize external interference. The microstrip antennas were positioned in close proximity to the bone samples, mimicking non-invasive diagnostic scenarios while ensuring the accuracy of signal transmission and reflection measurements. The study found significant correlations between the dielectric properties of the bone and the structural characteristics, such as porosity and density, which are critical indicators of bone health. Authors demonstrated the potential of RF technology for non-invasive bone health diagnostics and emphasized the role of natural bone samples in validating theoretical models and antenna designs. This research underscores the importance of combining such experimental approaches with more anatomically accurate representations, such as segmented 3D models, to bridge the gap between experimental validation and clinical applications.

Hybrid Phantoms for Multilayer Modeling Hybrid phantoms that integrate multiple layers to represent bone, muscle, and fat tissues have also been explored. [22] developed such a phantom using silicone and polymer composites to emulate the layered structure of a human arm. These phantoms were crucial in validating wearable RF devices for bone health diagnostics. By mimicking the heterogeneity of biological tissues, hybrid phantoms provide a more accurate platform for RF antenna testing and optimization.

While phantoms have significantly advanced RF-based bone diagnostics, their limitations highlight the need for anatomically accurate representations of bone structures. Segmented 3D bone models derived from high-resolution CT scans address this gap by capturing the intricate geometries and dielectric heterogeneity of cortical and trabecular layers. Unlike predefined or natural phantoms, segmented 3D models allow for patient-specific analysis, ensuring that RF systems are tailored to individual anatomical variations. These models also enable a comprehensive understanding of electromagnetic wave interactions with bone tissue, which is critical for optimizing antenna design and improving diagnostic accuracy. The transition to segmented 3D models marks a pivotal step in advancing RF technology for clinical applications, bridging the

gap between experimental setups and real-world scenarios.

By leveraging the strengths of phantoms and addressing their limitations through anatomically realistic models, researchers can ensure that RF-based systems achieve their full potential in revolutionizing non-invasive bone health diagnostics. This research aims to address these gaps by developing a novel antenna design optimized for interaction with anatomically realistic bone models, thereby bridging the limitations of existing methodologies. The following chapter outlines the methodology adopted to achieve these objectives, detailing the experimental setup, simulation protocols, and validation techniques employed in this study.

Chapter 3

Methodology

In this study, for early prognosis of conditions like osteopenia/ osteoporosis has been targeted to evaluate the strength and density of bones. this is dine by integrating the RF technology into the bone health assessment process. RF is preferred for its non-ionizing radiations and potential for accurate and real-time measurements. A systematic approach is followed to construct a highly detailed 3D bone model from CT scans data, aiming to accurately represent the complexities of real femur (Thigh) bone and design body matched antennas that are specifically designed to operate effectively when in close proximity to the human body. In the end a prototype is developed for the experimentation of antennas, with the bone placed in the middle.

Briefly, non-ionizing RF technology is utilized for real-time bone health evaluation, incorporating detailed 3D bone models created from CT scans. The study further intoduces body-matched antennas designed for optimal performance, near human tissue, validated through a working prototype.

3.1   3D Bone Model

To successfully reconstruct a 3D bone model from original CT scan data, the initial step involved data acquisition. To ensure the creation of a highly detailed and microstructurally accurate bone model, advanced image processing techniques for segmentation were employed to distinguish between the two distinct layers of the bone. This study utilizes a pheasant bone. Subsequently, appropriate dielectric properties were assigned to each segmented layer for accurate representation in the model. For the dielectric properties of each layer of bone we refer to the ϵ_r value in the literature.

3.1.1 Acquisition of Scans

This research involves rigorous data acquisition to develop a highly detailed and microstructurally accurate 3D bone model. Collaborating with the Great Britain's University of Manchester, UK; a comprehensive dataset of pheasant bone was accessed consisting of high-resolution CT scans generated using a 225 kV and 320 kV X-ray source Figure 3.1. These scans were captured at an exceptional resolution of 5 microns with the Nikon XCT facility, which provided unparalleled insights into the intricate architecture of the femur (thigh) bone. This precision imaging forms the basis for constructing an anatomically and structurally faithful model of Pheasant's femur bone. A staggering compilation of 1900 projections, where a single projection is shown in Figure 3.2, precisely encapsulates the femoral (Thigh) structure, providing a rich reservoir of data for our endeavors in bone health monitoring. Each scan provided a detailed voxel-based representation of bone morphology, hence creating critical insights into the density, mineral composition, and microstructural organization of bone. This high-resolution data enabled precise quantification of trabecular and cortical bone properties, to investigate an in-depth understanding of load-bearing capability, material heterogeneity, and the biomechanical implications of microstructural variations. Such data is pivotal for advancing the fields of bone health assessment, biomaterials research, and orthopedic applications using an interface of engineering and mathematical methods.
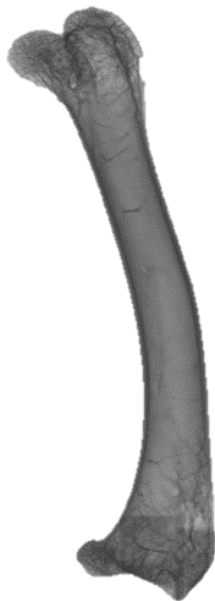

Figure 3.1: CT scan of Pheasant Bone

Figure 3.2: Single Projection

3.1.2 Image Processing

From raw scans to a refined 3D bone model, a meticulous process of data segmentation was employed. The imaging data acquired is stored in DICOM (Digital Imaging and Communications in Medicine) format, which is the standard format for medical imaging data. Each image slice is saved as a .dcm file, containing metadata that includes patient information, scan settings, and the actual image data. The .dcm files are imported into 3D Slicer, an open-source software platform for the analysis and visualization of medical images.

The DICOM Patcher module is used to ensure that all DICOM files are correctly formatted and compatible with 3D Slicer, facilitating a smooth import process. Utilizing the advanced capabilities of 3D Slicer Figure 3.3, a state-of-the-art segmentation platform known for its precision, the acquired CT data was carefully processed to segment distinct layers of bone. Each projection underwent a rigorous segmentation process, incorporating manual refinement to ensure accurate representation of the bone's microarchitecture. This methodical approach enabled the detailed characterization of cortical and trabecular structures, preserving critical morphological features essential for biomechanical and structural analyses. The Cortical layer, representing
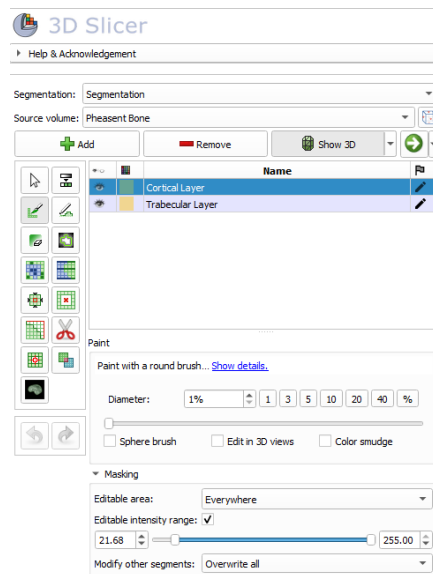

Figure 3.3: 3D Slicer Tool

the dense outer surface of the bone and the trabecular layer, comprising the spongy inner structure, were identified as key components during the segmentation process Figure 3.4. Each Layer was carefully segmented to accurately reflect the anatomical complexities of pheasant bone. This precise segmentation prcoess, forms the foundation

21

of our methodology, ensuring that the resulting 3D bone model faithfully represents the intricate geometry and microarchitecture of the scanned bone.
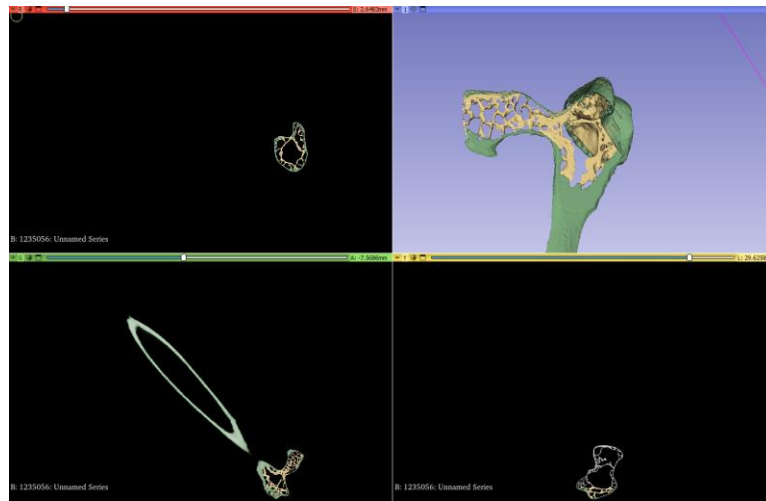

Figure 3.4: Segmented Layers

3.1.3 Image based modeling-A Smart Approach

Image-based modeling plays a key role in improving the efficiency and accuracy of data segmentation. In this particular approach, modern imaging techniques were combined with traditional methods to create a more effective method. The main focus of our method is the combination of thresholding and cropping techniques, which are designed to streamline the segmentation process. This combination enabled high accuracy and allowed a better reconstruction of detailed 3D models that closely represent the complexity of the selected bone. The Scissors tool in the Segment Editor is used to isolate a specific region of interest (ROI) within the bone Figure 3.5. By drawing a box around the desired area, typically the epiphysis (the rounded end of the bone), both the cortical and trabecular layers within this ROI was selected for further analysis. This ensured that the segmentation focused on the relevant anatomical features.

For segmenting two layers based on the source volume intensity range, a masking option was used from Threshold as it gives Editable intensity range and gives the paint effect that is required to trace the layers for segmentation. The Threshold tool Figure 3.6 was used to refine the segmentation by setting intensity ranges which corresponds to the different tissue types. By adjusting the editable intensity range, the tool highlights the areas that fall within these ranges, effectively "painting" the segments. This allowed for precise differentiation between the cortical and trabecular layers based on their density and intensity values in the imaging data.
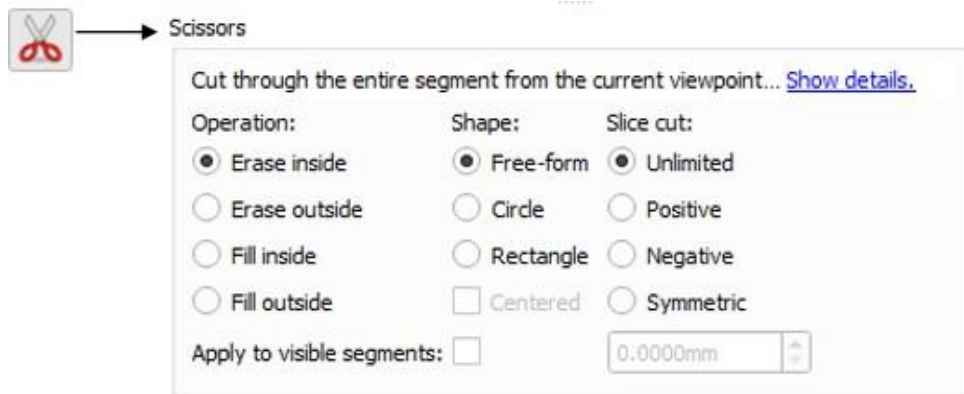
Figure 3.5: Scissors Tool

Segmenting them includes segmenting each projection of the selected ROI in all 3 dimensions separately. The segmentation process involved examining and refining the
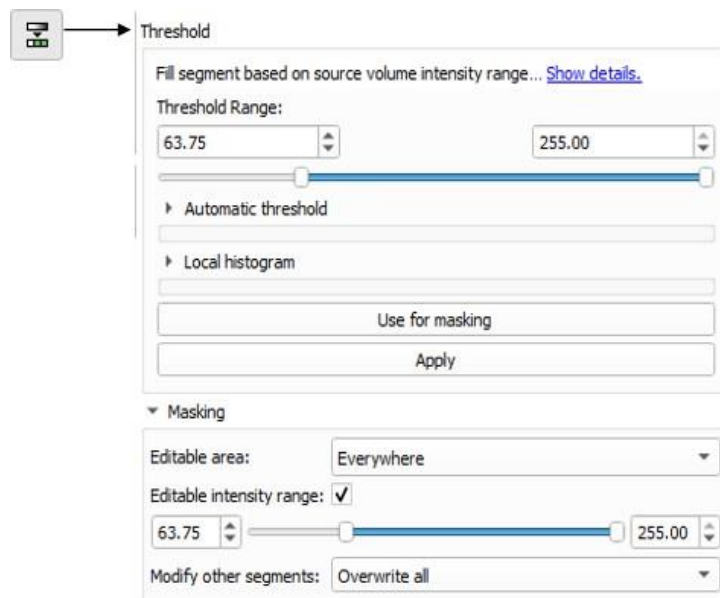
Figure 3.6: Thresholding Tool

segmentation in all three anatomical planes (axial, sagittal, and coronal). This ensured a comprehensive and accurate segmentation of the cortical and trabecular layers throughout the entire volume of the ROI , providing a detailed 3D representation of the bone structure. This innovative approach enhances the ability to extract critical bone segments with precision, going beyond the limitations of traditional segmentation

methods. By effectively navigating the complex microstructural terrain of bone, it enables a deeper understanding of bone composition and density, opening new avenues for advanced analysis and modeling. The final cropped and segmented 3D bone mode is shown in the Figure 3.7 below, where the yellow segmented part represents Trabecular bone (spongy/porous) and the green segmented part is the cortical bone part.

(a)   (b)

Figure 3.7: Reconstructed 3D Bone Model

3.1.4 Volume Rendering

Once the bone model was cropped and segmented in 3D Slicer software, the final model had to be in the solid form to perform simulations on it. In order to convert the segmented bone model to a solid model. Cortical and trabecular were exported into two separate files from 3D slicer in stl (stereo lithography) format Figure 3.8. A file format commonly used for 3D printing and computer-aided design (CAD).
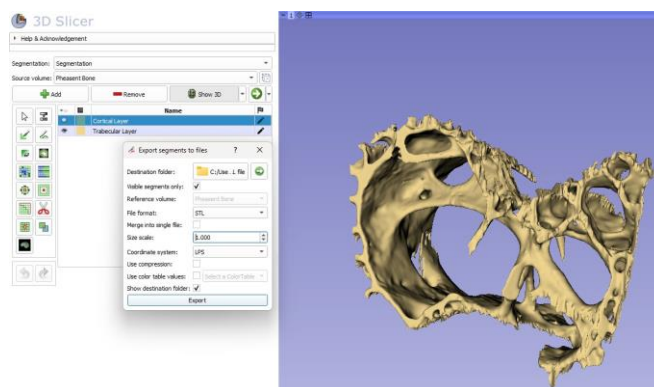
Figure 3.8: Exporting Trabecular Bone model from 3D Slicer

Later on, the bone model was exported into Autodesk Meshmixer. Meshmixer is a versatile 3D mesh editing software used for sculpting, refining, and preparing models for 3D printing, offering tools for mesh optimization, repair, and custom support generation.This software was used to convert the 3D bone model into a solid Figure 3.9(a), which helped in meshing and with the experiments later. Both the layers Cortical and Trabecular layer were converted into solids separately and exported in STL format as shown in Figure 3.9(b) to be then imported in to CST software.
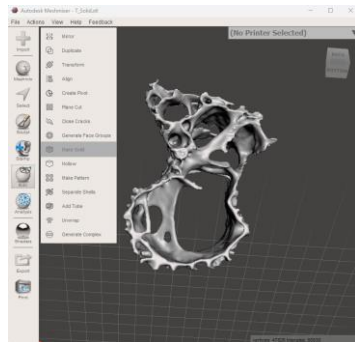
(a) Making Solid bone model   (b) Exporting solid bone model
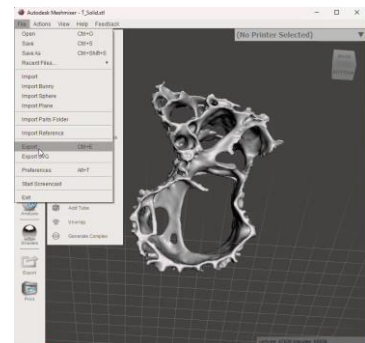
Figure 3.9: Converting the segmented bone into a solid in Blender software

3.1.5 Assigning Material Properties

After creating the 3D bone model and converting it into a solid structure, the next step involves assigning properties to ensure it closely matches real bone.

Figure 3.10: Bone Model in CST Software

25

Specific dielectric properties ϵ_r are assigned to each segmented bone layer, which helps the virtual model accurately represent the bone's material. These dielectric values are selected based on data from scientific studies, ensuring the model reflects the true characteristics of bone. The electromagnetic properties o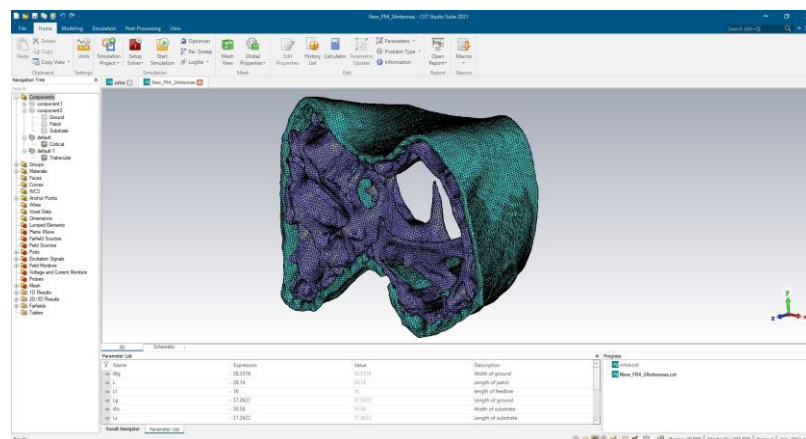f the reconstructed model now mirror those of real bone tissue. For assigning properties , model was imported in (Computer Simulation Technology) CST Software Figure 3.10, the same software in which antennas were designed. When the model was imported into CST software, its size was very small as compared to the size of the antennas. The model was from the Transforming module, scaling option was selected to improve the size of bone in comparison to the antennas.

To edit the material property, select the component and from drop down menu select "edit the material property". From the literature acquired values were Epsilon ϵ_r and Electrical Conductivity. For the Cortical bone $\epsilon_r = 12.4$ and El. conductivity = 0.145[S/m] as shown in fig 3.11.
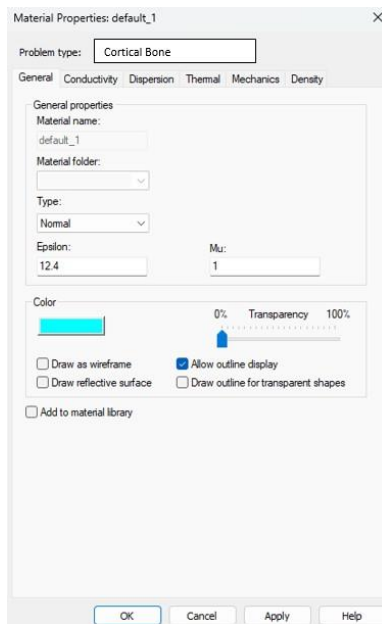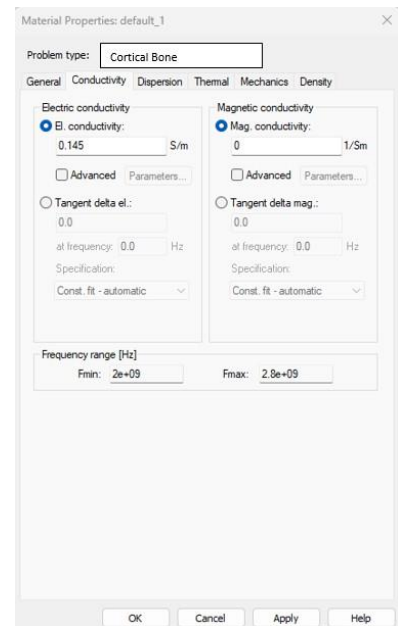
| (a) | (b) |

Figure 3.11: Assigning Properties to Cortical Bone

For Trabecular bone $\epsilon_r = 20.8$ and El. conductivity = 0.344[S/m] as shown in fig 3.12. This process of property assignment served as the key player of our methodology, facilitating the simulation of realistic interactions between RF signals and bone tissue. As each layer assumes its unique electromagnetic signature, 3D bone model emerges as a beacon of fidelity, to revolutionize the field of bone health monitoring.
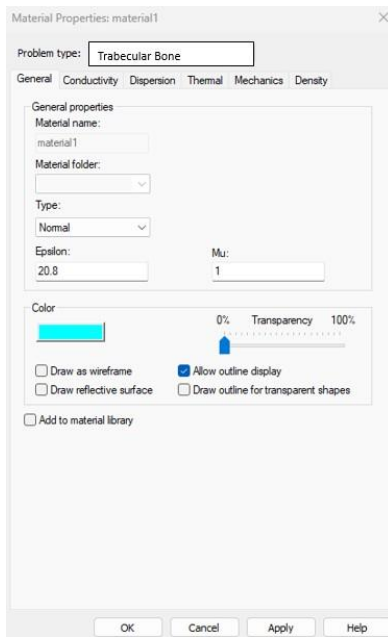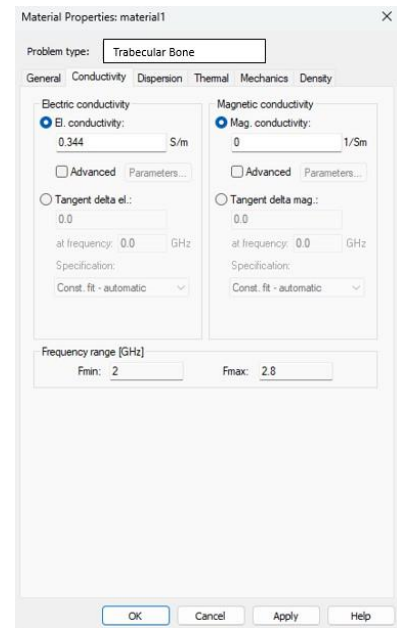
(a)	(b)

Figure 3.12: Assigning Properties to Trabecular Bone

After assigning the material properties, density values were assigned to the segmented Cortical bone and trabecular bone. Density is an intrinsic property, represented as (Rho) that links the geometric model to mass, enabling calculations of stress distribution, and SAR (specific Absorption Rate) analysis. For our 3D bone model

Figure 3.13: Cortical Bone

with distinct cortical and trabecular layers, we define separate density values in light of work done in [38], reflecting the physiological differences between both the regions, enhancing the model's fidelity. The cortical layer, being denser and mechanically robust, requires a higher density value of $2000 \, \text{kg/m}^3$ to represent its structural function

effectively Figure 3.13.

Conversely, the trabecular layer, characterized by its spongy, porous architecture, has a lower density of $1000\,\text{kg/m}^3$ as shown in Figure 3.14, consistent with its role in absorbing shocks and supporting metabolic activities. By assigning accurate density values to each layer, the model not only achieves a realistic mass representation but also becomes capable of yielding precise outcomes in simulations, whether for research, diagnostics, or therapeutic SAR analysis.

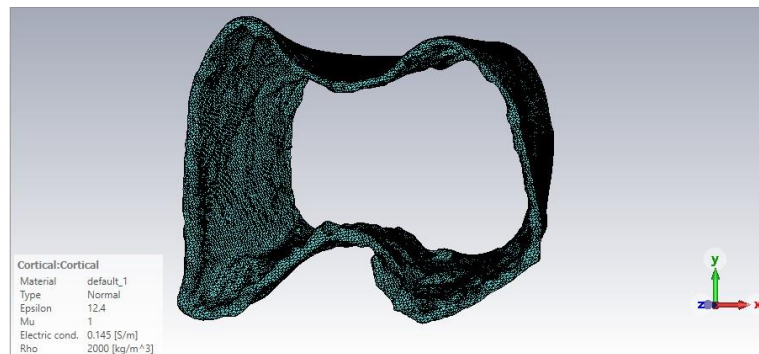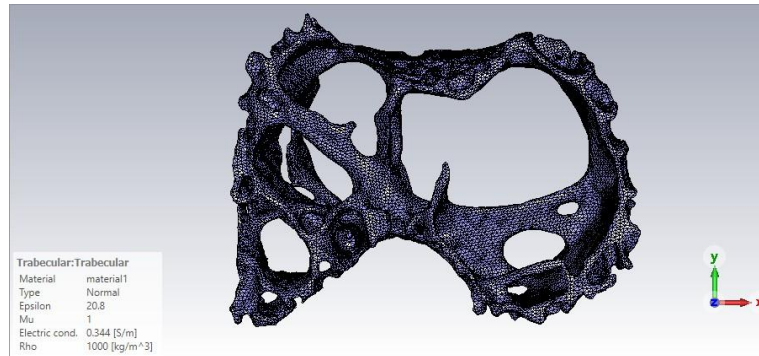Figure 3.14: Trabecular Bone

3.2 Antenna Design

One of the primary objectives of this research was to design on-body matched antennas suitable for operation in close proximity to the human body. Antenna is intended for medical applications, specifically for RF-based bone health analysis, operating within the Industrial, Scientific, and Medical (ISM) band specifically at 2.45 GHz. At higher frequencies, penetration depth decreases, making them better suited for thinner bones or peripheral regions like the wrist or fingers, as indicated in previous research. The 2.45 GHz frequency, commonly employed in medical applications due to its presence in the ISM band, has been shown to produce reliable results in bone tissue analysis. This is supported by numerous studies, including those that validated microwave sensing prototypes for evaluating bone health [39, 40].The design of this antenna involves several key considerations to ensure optimal performance and integration with the human body.

3.2.1 Design Considerations

1. ***Compact Size and Low Profile***: The antenna to be designed had to be compact and with a low profile to facilitate on-body placement. A small, lightweight

design ensured that the antenna can be comfortably worn without interfering with the user's daily activities or movements. This was crucial for continuous health monitoring applications, where user comfort and ease of use was the top priority. There are studies that collectively underscore the critical role of compact antenna design in the advancement of wearable devices for non-invasive health monitoring, as in [18, 41]

2. ***Efficient Radiation Characteristics***: The antenna must exhibit efficient radiation characteristics, specifically in the near-field region. Effective transmission and reception of electromagnetic signals are critical for accurate bone health analysis. Hence, near-field performance of this antenna was particularly important as the signals need to penetrate the body tissues and interact with the bones to provide reliable diagnostic information.

3. ***Matched Impedance***: To maximize power transfer and minimize signal reflection, impedance matching was an essential step. Especially when the antenna had to operate in close proximity to the human body. The human bone is geometrically complex, therefore it is a lossy medium that can significantly affect the antenna's performance. The antenna's performance is highly influenced by impedance mismatches. Consequently, precise impedance matching was necessary to optimize the antenna's efficiency, minimizing signal loss and reflection.

3.2.2   Technical Specifications

1. **Operating Frequency**: The antenna was designed to operate within the ISM band at 2.45 GHz. As highlighted by authors in [42, 43], this frequency is widely used in osteoporosis detection due to its optimal balance of tissue penetration and resolution, enabling non-invasive assessment of bone mineral density (BMD). Its inclusion in the ISM band allows for cost-effective, portable applications.

2. **Substrate Selection**: The choice of substrate for the antenna was taken into account, considering loss tangent, dielectrical properties, and flexibililty. In [44] Rogers RT/duroid 5880 substrate, was selected due to its low dielectric constant and low loss tangent. Number of research works have explored their use in biomedical applications within the 2.4–2.5 GHz ISM band. As from [45] findings reveal that the antenna made with Rogers 5880 delivers superior gain and efficiency. Such features are especially valuable for antennas operating near human bone tissue, as they help minimize signal degradation and ensure consistent performance.

3. **Simulation and Testing**: Advanced simulation tools, such as CST Microwave Studio, HFSS are mostly used to model and optimize the antenna design. Simulations help in predicting the antenna's performance in the presence of the human

body and in various usage scenarios. Prototype testing was conducted to validate the simulation results.

By addressing these design considerations and technical specifications, various antenna designs were considered and the best two antennas were designed and developed for an on-body matched RF-based bone health evaluation application, with optimized parameters. Aiming to achieve a balance between performance, user comfort, and practical application in medical diagnostics.

3.2.3 Proposed Design and Dimension

Two identical rectangular microstrip patch antennas were designed using CST software, which were compact in size and easy to manufacture, making them suitable for body applications. A Rogers RT/Duroid 5880 substrate with a thickness h of 1.57 mm was used. The substrate has a dielectric constant ϵ_r = 2.2. The patch itself was made of copper with a thickness t = 0.035 mm. One of the antennas was operating as a transmitter and the other as a receiver. The structure of the antennas was chosen to resonate in ISM band. The design of antenna is shown in Figure 3.15 and dimensions of the antenna are shown in Figure 3.16 and given in Table 3.1 respectively.

(a)　　　　　　　　　　　　　　　　　(b)
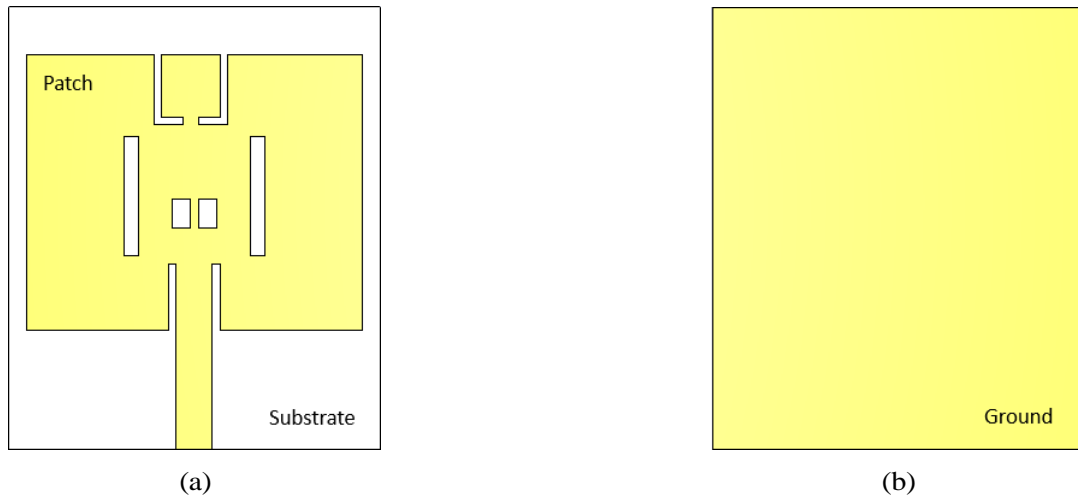
Figure 3.15: Antenna Design

Width of the feedline (Wf) of an antenna is carefully chosen to match the characteristic impedance of the system, which is commonly 50 ohms. Impedance matching is an important step while designing an antenna in order to minimize reflections of electromagnetic waves back to the source, which then results into reduced efficiency. Efficiency is the measure of how effectively antenna radiates the power supplied in form of electromagnetic waves, compared to any losses caused due to factors like dielectric losses,
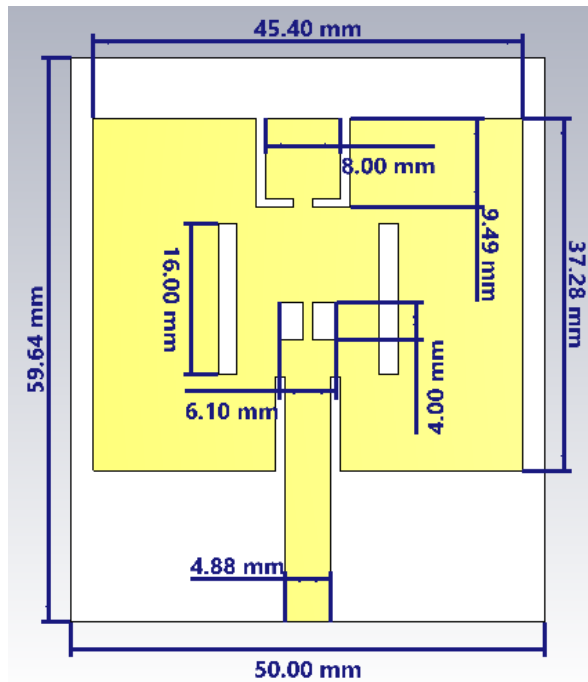
Figure 3.16: Dimensions of the Antenna

Table 3.1. Design Parameters for Microstrip Patch Antenna

Parameter	Parameter Name	Calculated Value (mm)
Wg	Width of ground	50
Lg	Length of ground	59.64
W	Width of patch	45.40
L	Length of patch	37.28
hs	Height of substrate	1.57
hc	Height of copper clad	0.035
Wf	Width of feed	4.88
Lf	Length of feed	16

and mismatching. CST provides tool "Macros" to calculate the exact feedline width to ensure proper impedance line matching as shown in Figure 3.17 below. From the drop down menu "Calculate analytical Line Impedance" was selected Figure 3.18. Thin

31
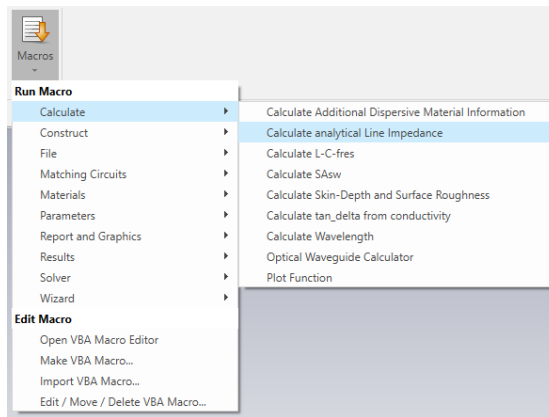
Figure 3.17: Macros Tool

microstrip was chosen and values were entered, such as operating frequency 2.45GHz, dielectric constant $\epsilon_r = 2.2$ of substrate, and thickness h of 1.57. By changing the width, the input impedance Z_O at 50 Ohms was achieved. After adjusting the width
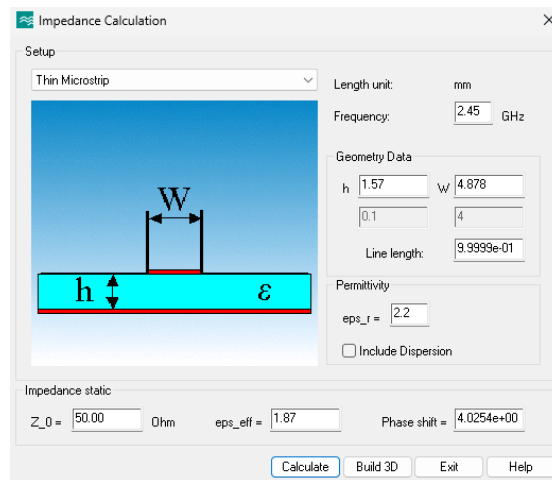
Figure 3.18: Impedance Calculation

of feedline, a waveguide port is assigned to excite the antenna structure as a source of electromagnetic waves through the transmission lines. It is often placed at the end of a microstrip feed line in planar antenna designs. The dimensions of the port are typically set according to the size of the feedline and boundary conditions are defined to excite the specific fields for propagation. Using the "Pick" tool,shown in Figure 3.19 select the face, width of feedline

When the face is selected, next step is to assign waveguide port. From the simulation menu we select the "Waveguide port" option. A window appears in which we assign the values Xmin, Xmax, Zmin, and Zmax as shown in Figure 3.20

32
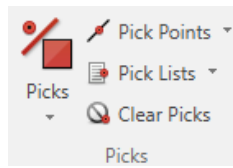
Figure 3.19: Pick Tool
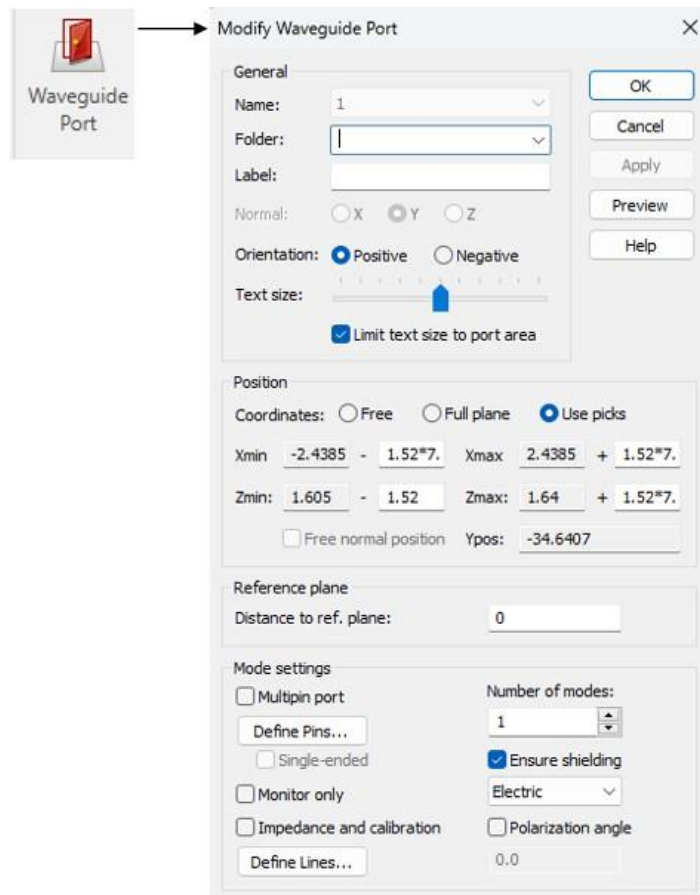
Figure 3.20: Waveguide Port Assignment

Once the width of feedline is set and waveguide port assigned, a red box indicating the input port (1) is visible at the bottom of the antenna as shown in the Figure 3.21.

3.2.4 Antenna Geometry Specifications

In order to evaluate the bone model, two identical antennas are strategically positioned on opposite sides. Face-to-face alignment ensures maximum interaction of the electromagnetic waves with the bone model reducing the probability of scattering and
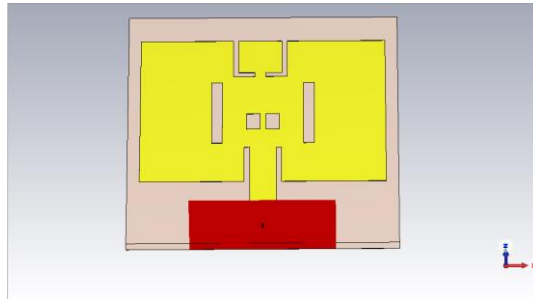
Figure 3.21: Port 1 Assigned

dispersion of signals. One antenna functions as the transmitter, while the other antenna serves as the receiver. To construct this arrangement, first duplicate the geometry of the antenna 1 using the transformation tool in CST as shown in Figure 3.22.
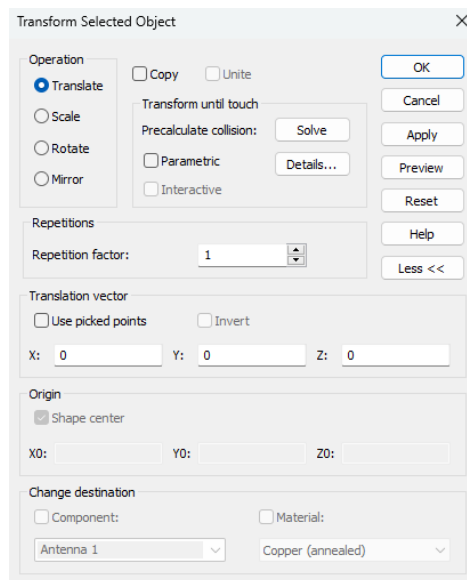
Figure 3.22: Transform Tool

The duplicate antenna was shifted along x-axis to ensure the correct distance between the two antennas. After adjusting the orientation, Antenna 1 was rotated 90 degrees along the y-axis, while Antenna 2 wwas rotated at -90 degrees along the same axis. Both antennas were positioned to face each other with an initial distance of 50mm along the x-axis. Once the alignment was set, Antenna 1 was assigned port 1 (transmitter) and Antenna 2 was assigned port 2 (receiver). The geometry is shown in Figure 3.23 shows the geometry.
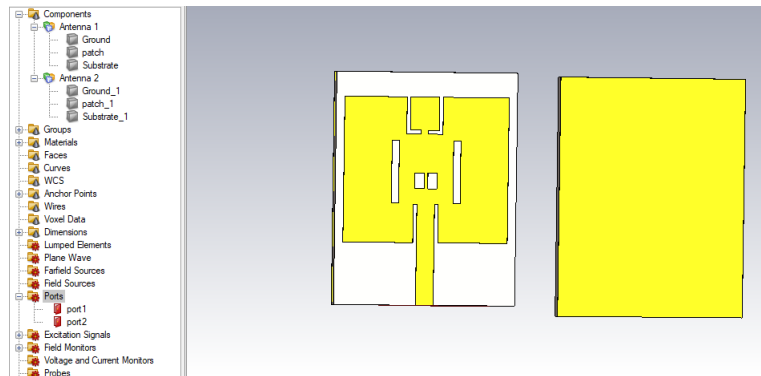
Figure 3.23: Geometry of 2 Antennas

3.2.5   Simulation Setup & Configuration

Following the antenna configuration, the bone model was imported into the system. Using the import/export option from the modeling tool, 3D files in .stl format were successfully imported, as shown in Figure 3.24. The study aimed to investigate the influence of distinct dielectric properties on the propagation of electromagnetic waves through the bone model. The attenuation, phase shift, and reflection of the waves were analyzed to differentiate between healthy and unhealthy bone tissues.
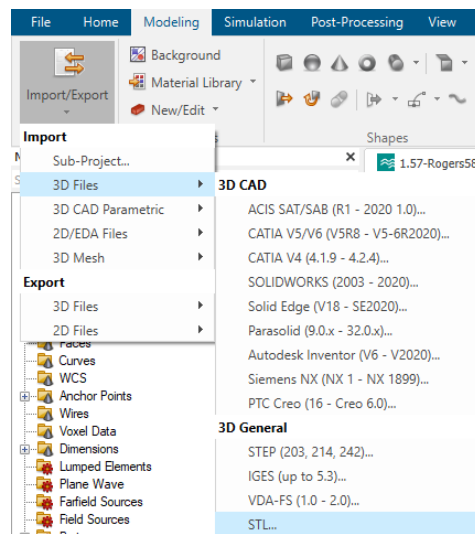
Figure 3.24: Importing 3D Files

As the transmitted signal from Antenna 1 interacted with the bone model, which included both the cortical and trabecular layers, it underwent changes. These variations were detected at the receiving end, providing key insights into the bone's composition

35

through the evaluation of attenuation, reflection, and transmission losses. The bone configuration with antennas is illustrated in Figure 3.25

Figure 3.25: Antennas with Bone Configuration

3.2.6 Antenna Fabrication Process

Once the antenna design has been optimized and simukated in CST, with all paramters such as dimensions, substrate material, and performance characteristics thoroughly refined, the design finalized for fabrication. Initial step in thus process involves exporting the layout as Gerber files, a widely accepted standard for printed circuit board (PCB) production. These files contain critical information, including the antennas's shape and the precise locations of the slots within the PCB layout. These gerber files are then correctly formatted and uploaded to the **LPKF machine**. This machine selects the appropriate tools for the **fabrication of antenna** while configuring the parameters for etching. At the end, fabricated antenna undergoes **soldering and testing**
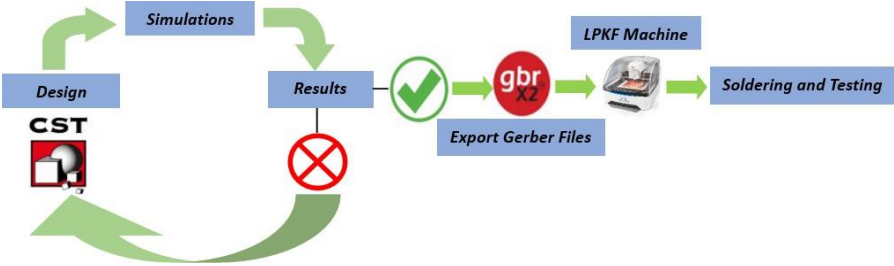
Figure 3.26: Antenna Fabrication Cycle

where SMA (coaxial RF) connector with an impedance of 50 Ohms is soldered to the

end the antenna's feedline. SMA connector then helps to connect the VNA cable to the antenna; to evaluate the performance parameters such as return loss (S11), gain, and radiation patterns to ensure the antenna functions as expected. The design cycle for fabrication is shown in the Figure 3.26.

Upon finalizing the antenna design in CST software, Gerber files for the ground and patch were exported to the LPKF machine, adhering to the previously outlined design cycle. This facilitated the successful fabrication of the antennas, as depicted in Figure 3.27. The subsequent phase involves testing , with the results presented in the "Result & Discussion" chapter.
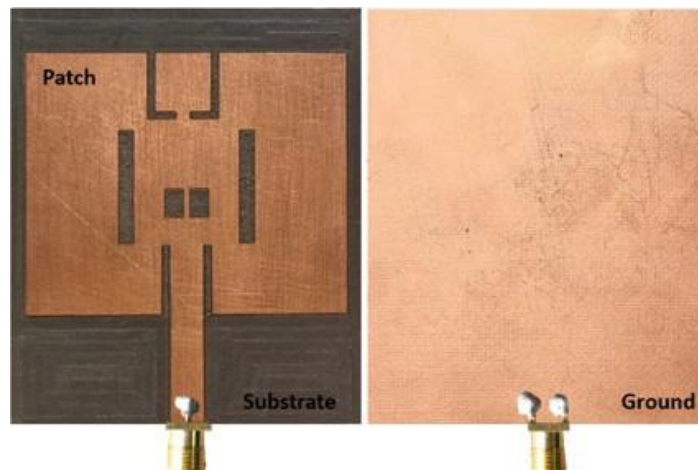
Figure 3.27: Fabricated Antennas from LPKF Machine, with soldered SMA connector

3.3 CAD Modeling

As previously discussed, Dual-Energy X-ray Absorptiometry (DEXA) scans are widely utilized medical imaging technique for assessing bone density and diagnosing conditions such as osteoporosis. Before the scanning process, CAD modeling is often employed to simulate and optimize the bone structure in order to improve diagnostic accuracy. The DEXA process involves emitting two X-ray beams at different energy levels, which pass through the body and are absorbed differently by bone and soft tissues. Then a detector measures the amount of each X-ray beam that passes through the body, and the machine calculates the bone mineral density (BMD) by comparing the absorption levels of the two beams. This difference in absorption then allows the machine to determine the density of the bone. Despite its effectiveness, there are limitations in these traditional methods, including exposure to ionizing radiations, and potential shortcomings in capturing true bone health. Additionally, the presence of soft tissue, and machine calibration can also affect the accuracy of DEXA scans. In this situation Radio Frequency (RF) technology offers a ray of hope, a non-invasive approach that could provide a more comprehensive picture of bone health.

3.3.1 Conceptual Model

Initially study was focused on a conceptual model for bone health monitoring in a non-invasive manner using RF technology, that had been designed for a visual representation of the idea. Where, two antennas were strategically placed on either side, with a cork model nestled in the middle as shown in Figure 3.28.
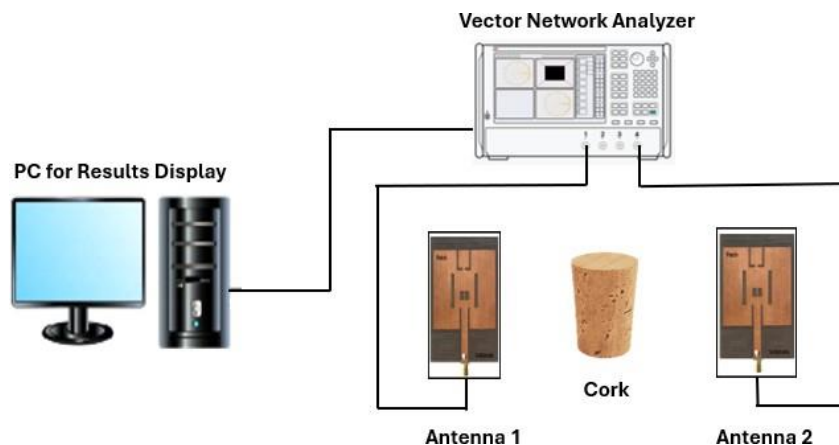
Figure 3.28: Conceptual Model

This figure illustrates: **Patch Antennas (1 and 2)**: Two antennas were positioned on either side of the bone model to emit and receive RF signals. The bone was placed

between these antennas to evaluate its health within the targeted area by capturing the signals that interacted with the bone. **Vector Network Analyzer**: This device measured RF signal parameters, such as the reflection coefficient and transmission coefficient, as the signals passed through the bone. It analyzed changes in the RF signals caused by their interaction with the bone tissue, providing valuable data for assessing bone health. **PC for Results Display**: A computer was used to process and display the results obtained from the vector network analyzer. It provided a user-friendly interface for visualizing the bone health data and analyzing the outcomes of the RF-based evaluation **Cork**: A cork model was used as a substitute for the bone because it is also a composite porous material similar to the bone. The cork model is placed between the two patch antennas to analyze the results during testing.

This conceptual model was the testing ground for the innovative RF-based approach to bone health assessment. On the basis of this conceptual model a prototype system was developed.

3.3.2 CAD Design & Prototype

The prototype system was designed and modeled within SolidWorks, a 3D computer-aided design (CAD) software. This prototype prioritizes functionality to facilitate precise experimentation. It features two antenna holders and a dedicated holder for the bone model. The platform base incorporates a crucial element, a scale of 100 cm for precise back-and-forth movement of the antennas. This adjustability allows for thorough control over antenna positioning during experiments, ensuring optimal signal interaction with the bone model for data collection. The CAD models are shown in the Figure 3.29. The initial prototype design prioritized simplicity for efficient devel-

(a) Antenna Holder   (b) Bone Holder   (c) Platform
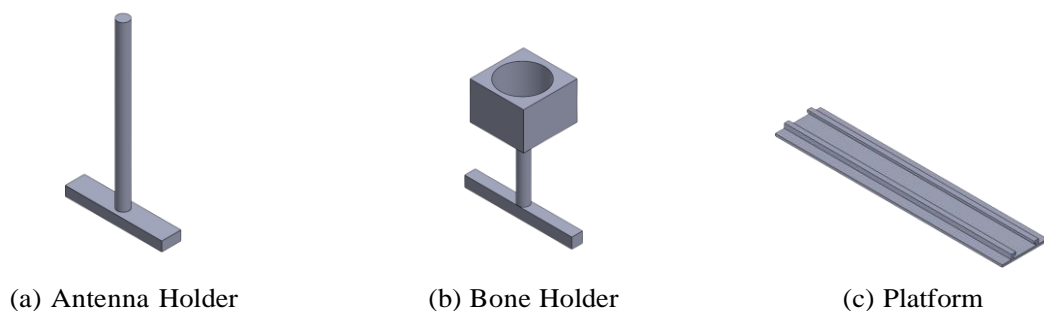
Figure 3.29: CAD Models

opment and testing. To minimize potential signal interference from the bone holder itself, its length was reduced, ensuring only the bone specimen is directly in front of the antennas. For adjustable antenna positioning, the antenna holders utilize a zip-tie mechanism, allowing for variations in antenna height during experimentation.

The bone holder itself incorporates a versatile design with a diameter wide enough to accommodate bones of varying thicknesses. The prototype was printed using a 3D printer, Ultimaker installed in Makers Lab at SINES. It was employed for the fabrication of the prototype components, such as bone holder and antenna holder. Tough PLA filament with a diameter of 2.85 mm was chosen as the printing material due to its durability and suitability for functional prototypes. Approximately 150 grams of filament were used to print the entire setup. The platform base, featuring rails on the sides to facilitate smooth movement of the antenna holders, was sourced from a local vendor. Final experimental setup in CAD vs the actual setup are shown in the Figure 3.30.
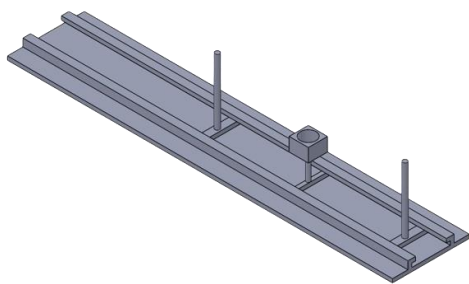
(a) Solidworks CAD Model   (b) 3D Printed Prototype
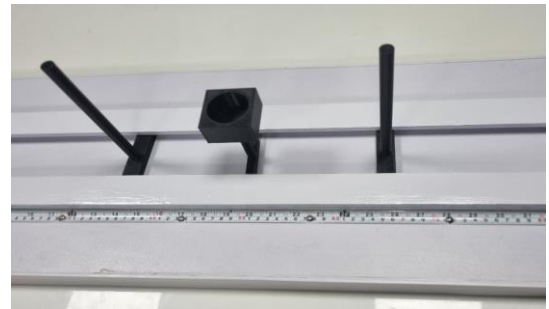
Figure 3.30: Experimental Setup

The CAD modeling process played a crucial role in visualizing and refining the prototype design. SolidWorks allowed for detailed planning and simulation of the components, ensuring that each part fit together seamlessly. This pre-fabrication step helped identify potential design flaws and provided an opportunity to make necessary adjustments before printing. The CAD models were carefully constructed with accurate dimensions and features, ensuring that the physical prototype would function as intended. Detailed renderings and animations of the model facilitated a clear understanding of the design concepts. The successful creation of the prototype allowed for the progression to experimental testing and data collection. In conclusion, the integration of SolidWorks for CAD modeling was crucial to the development of the RF-based bone health evaluation prototype, culminating in a functional and effective system ready for validation through experimentation.

Chapter 4

RESULTS & DISCUSSION

4.1 CST Simulations for Antenna

4.1.1 Performance Characteristics

The antenna design was simulated using electromagnetic simulation software (e.g., CST Studio Suite) to analyze its performance characteristics. Parameters such as return loss, radiation pattern, and efficiency are evaluated to assess antenna performance and suitability for on-body operation. Where, **Return Loss** is a measure of the reflected power from the antenna compared to the incident power. It indicates how well the antenna is matched to the transmission line, with lower values signifying better impedance matching and minimal signal reflection. **Radiation Pattern** describes the distribution of radiated power from the antenna in space. It provides insight into the directionality and coverage area of the antenna, which is crucial for ensuring effective signal transmission and reception in on-body applications. And **Efficiency** refers to the ratio of the power radiated by the antenna to the total input power. It accounts for losses due to impedance mismatch, material absorption, and other factors, indicating the effectiveness of the antenna in converting input power into radiated electromagnetic waves. Iterative optimization techniques were employed to fine-tune the antenna design to meet the specified requirements. S-parameters or the scattering parameters provide a convenient and comprehensive way to characterize the relation between the input and output signals. S11 is the reflection coefficient. It can be seen that S11 of -20.9704 dB has been achieved at 2.45 GHz which is below the standard -10 dB line, fig 4.1 shows the S11 parameter of the simulated antenna. The gain of the antenna at
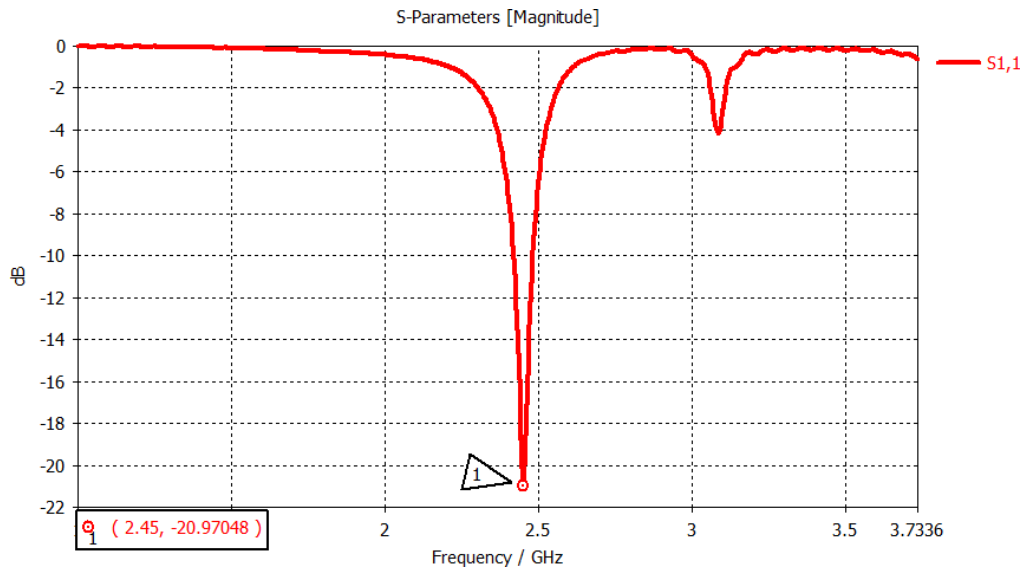
Figure 4.1: s11 parameter of the simulated antenna

2.45 GHz is 3.051dB as shown in fig 4.2. The choice of antenna gain depends on the specific requirements of the communication system or application, as it involves trade-offs between directional performance and coverage. In order to achieve high radiation
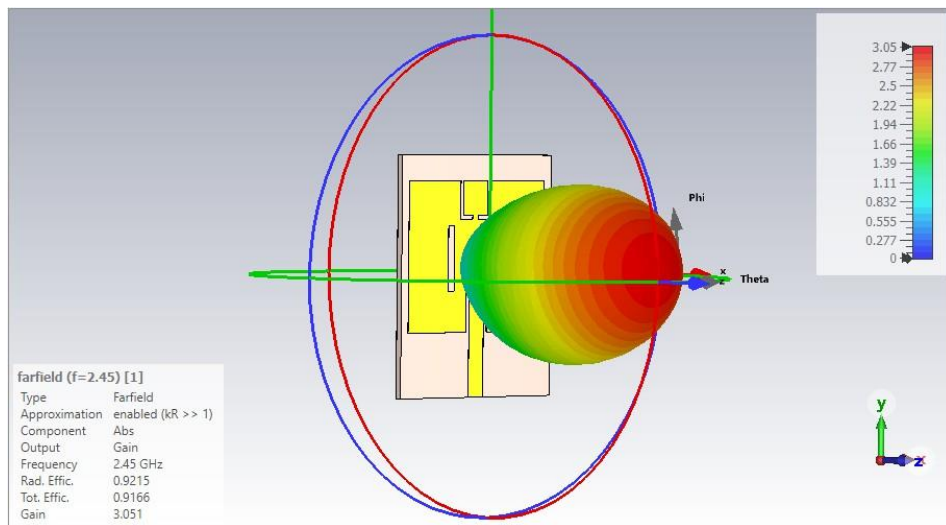
Figure 4.2: Gain of Antenna

and total efficiency substrate of low dielectric constant $\epsilon_r = 2.2$ was used, so there can be minimum number of losses. Other than that slots were introduced in the geometry. The total efficiency achieved was 91.6 % at 2.45GHz as shown in Figure 4.3 .It can vary after optimizing the antenna. High radiation efficiency indicates minimal power loss within the antenna itself. This means that most of the electrical power delivered to the antenna gets converted into radiating electromagnetic waves. Conversely, a low radiation efficiency suggests significant power loss.
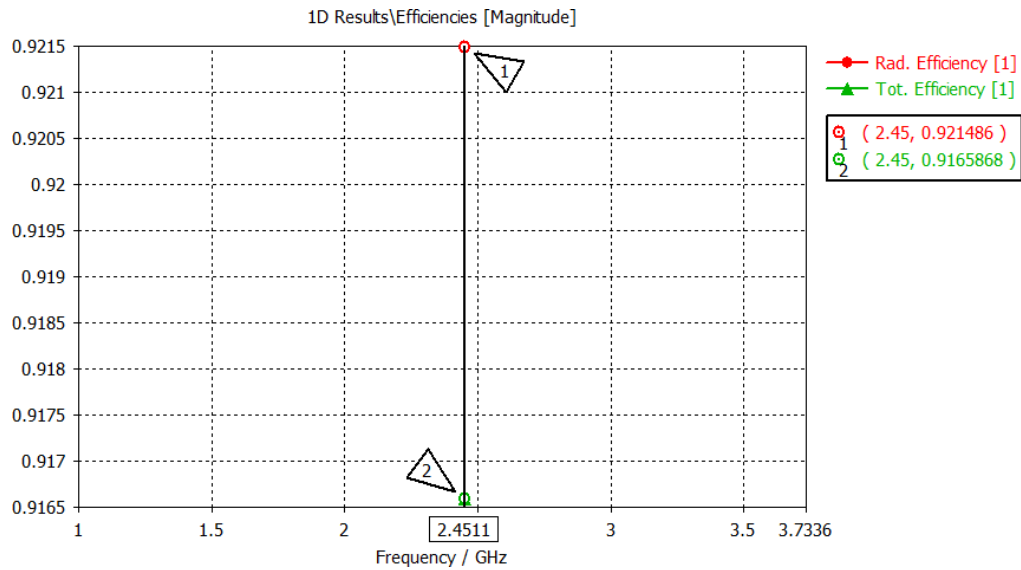
Figure 4.3: Radiation and Total Efficiency of Antenna

The parameter Voltage Standing Wave Ratio (VSWR) is the measure of how efficiently electromagnetic power is transmitted from a power source (VNA), through a transmission line, into the antenna. It indicates the quality of the impedance matching between the antenna and the transmission line.

Mathematically,

$$\text{VSWR} = \frac{V_{\text{max}}}{V_{\text{min}}}$$

Ideal ratio is 1 : 1, indicating perfect impedance matching, e.g., a 50 Ω transmission line to a 50 Ω antenna. A higher value of VSWR indicates mismatching, where more power is reflected back, leading to lower efficiency. An acceptable value is VSWR < 2, and the proposed antenna achieved VSWR = 1.19, as shown in Fig.4.4 below.
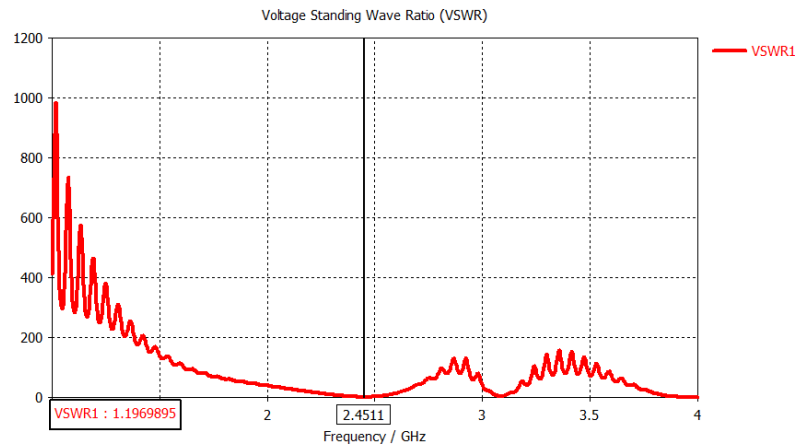
Figure 4.4: VSWR of Antenna

4.1.2 Antenna Model

The initial phase of testing involves observing the performance of the microstrip patch antennas placed in a face-to-face configuration at a distance of 50mm without any intervening medium in between, as shown in Fig 4.5. The measured S-parameters helped in understanding the baseline performance of the antennas in free space. The
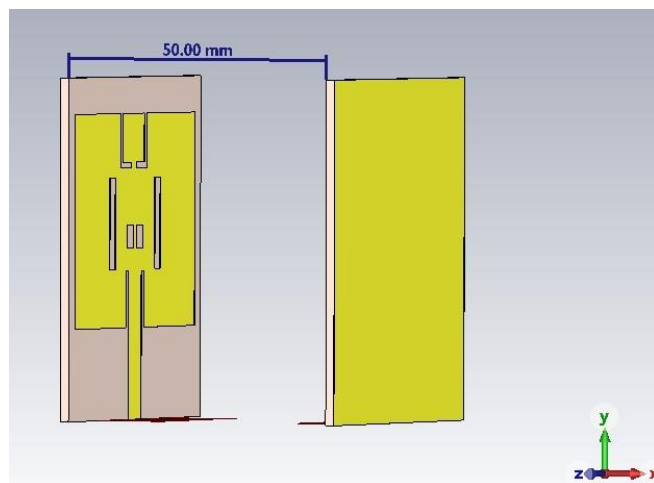
Figure 4.5: Configuration of microstrip patch antennas with a separation distance of 50mm, demonstrating a free-space interaction without bone model

results of the reflection coefficient (S11) and transmission coefficient (S21) as shown in Fig. 4.6, indicate that the interaction between the two antennas in their current configuration has shifted the operating frequency from 2.45GHz to 2.59GHz and altered the performance parameters, when placed at a distance of 50mm. The frequency shift
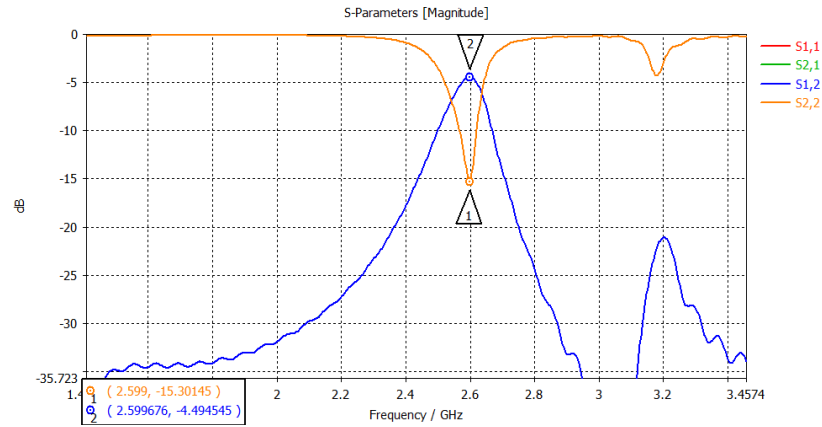
Figure 4.6: Without bone model

observed is likely caused by enhanced mutual coupling of electromagnetic fields between the two antennas, as a result of operating in proximity and their orientation. At 2.59GHz value of the reflection coefficient S11 = -15dB, indicates reduced impedance matching because of the near-field interactions between the antennas. On the other hand, the value of S21 = -4dB indicates strong transmission from antenna 1 to antenna 2, which implies that most of the transmitted power of the antenna is reaching the receiver end with minimal losses.

4.1.3   Antenna Simulation with Bone Model

Subsequent simulations involved placing a segmented 3D bone model, as shown in Figure 4.7.

This configuration of both antennas bone model is representative of the human wrist, as a dielectric medium between the antennas to evaluate changes in operating frequency and s-parameters in the CST software. After placing the bone model in the center between the antennas, the s parameters s11 and s21 were analyzed again, considering that s22 and s12 have the same value in case of identical antennas, to evaluate the difference caused by placing a complex bone model as a dielectric medium. Figure 4.8 illustrates these parameters as a function of frequency. This indicates how much power is reflected back to antenna 1 due to impedance mismatch. In the presented graph, two data markers are used to identify key parameters, where marker 1 represents the s21 or s12 parameter, which indicates the transmission coefficient, while marker 2 corresponds to the s11 or s22 parameter, reflecting the reflection coefficient. The graph highlights the impact of placing the bone model at a distance of 50mm from the antennas. When compared to the baseline measurements of antennas without the bone model, the placement of the bone caused significant deviations in the s-parameters. Initially, s11 was measured at -15 dB, and s21 was -4 dB at 2.59 GHz. With bone

45

Figure 4.7: Bone model positioned at the center, 50 mm from each antenna, with a total separation of 100 mm between Antenna 1 and Antenna 2

Figure 4.8: s11 and s21 parameters for the setup with the bone model placed centrally between the two antennas, highlighting the reflection and transmission characteristics of the system

placed at 50 mm, s11 increased to -12 dB, and s21 reduced to -8.6 dB, indicating increased reflection and reduced transmission.

4.1.4 Sensitivity Analysis based on Varying Distances

For sensitivity analysis, bone model was placed at different distances from both antennas, for example **100 mm**, and **150 mm** to clearly indicate distinct changes in the values of s21 and s11, illustrating the influence of the bone model on signal propagation and reflection. To demonstrate, in Figure 4.9 bone model was placed at a distance of **100mm** from both antennas, creating a total distance of **200mm** between antenna 1 and antenna 2
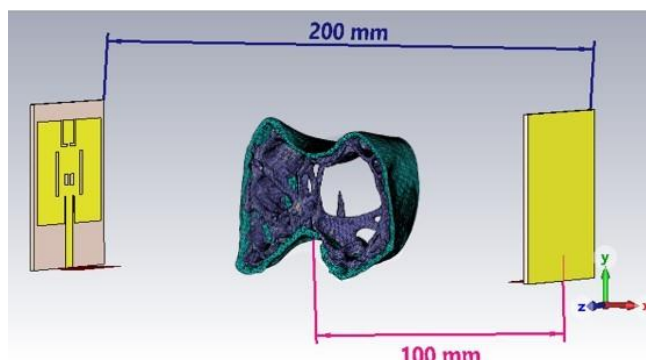
Figure 4.9: Bone model positioned at the center, 100 mm from each antenna, with a total separation of 200 mm between Antenna 1 and Antenna 2

After simulation, the influence of varied distance in scattering parameters was compared to the baseline measurements without the bone model, the increase in distance caused significant deviations in the s-parameters. At a distance of **50mm** bewtween both the antennas and without bone model, s11 was measured at -15 dB, and s21 was -4 dB at 2.59 GHz. With the bone placed at **100 mm** as shown in Figure 4.10, distance from both antennas, s11 decreased to -14.16 dB, and s21 reduced to -14.42 dB, indicating decreased reflection and reduced transmission. A dip of -6dB is measured in s21 parameter at **100 mm**, whereas both the s-parameters are at the same frequency of 2.60GHz only a minimal frequency shift is observed in s21 parameter.
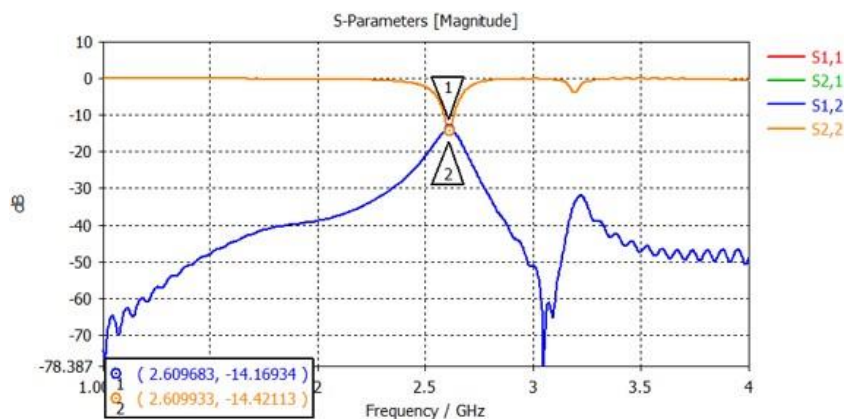
Figure 4.10: s11 and s21 parameters for the setup with the bone model placed centrally between the two antennas, highlighting the reflection and transmission characteristics of the system

Lastly, for the simulation of both the antennas segmented 3D bone model, the distance was set at a total distance of **300mm** and **150mm** at each side from the bone model, as shown in Fig. 4.11.
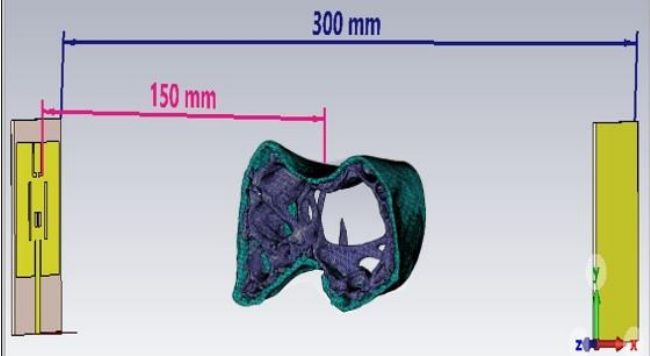
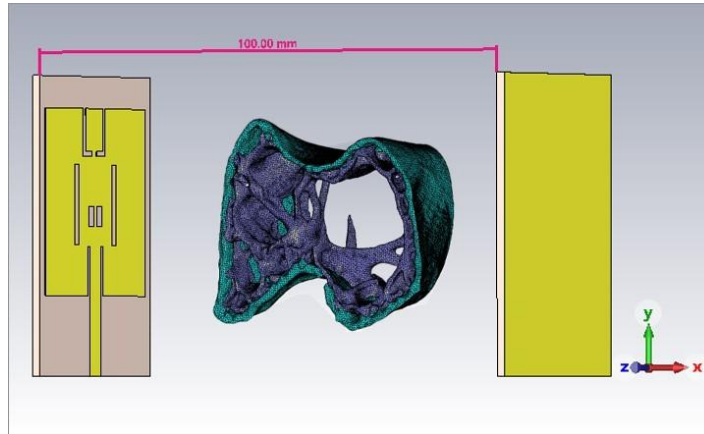Figure 4.11: Bone model positioned at the center, 150 mm from each antenna, with a total separation of 300 mm between Antenna 1 and Antenna 2

As a result for this configuration, graph in Figure 4.12 highlights the effect of distance on the measurement by placing the bone model at a distance of **150mm**. Bone's proximity can detune the antenna's performance. However, as the distance increases, electromagnetic waves interact with bone and the surrounding environment, causing losses leading to additional losses. In comparison to the basic simulation , where there was no dielectric medium in between the antennas, s11 was measured at -15 dB, and s21 was -4 dB at 2.59 GHz.
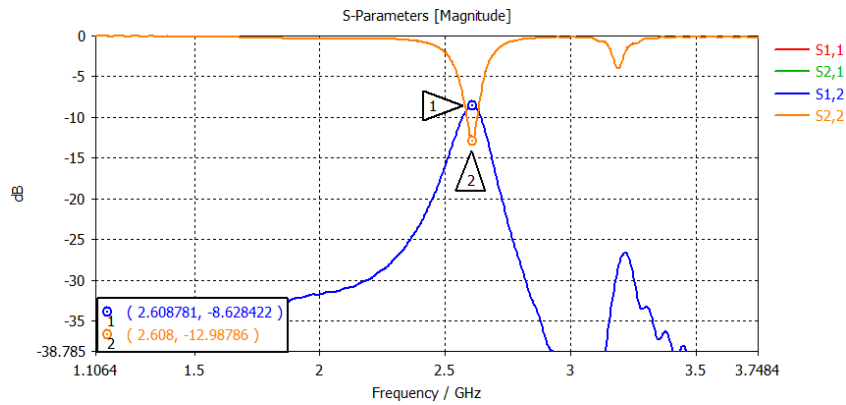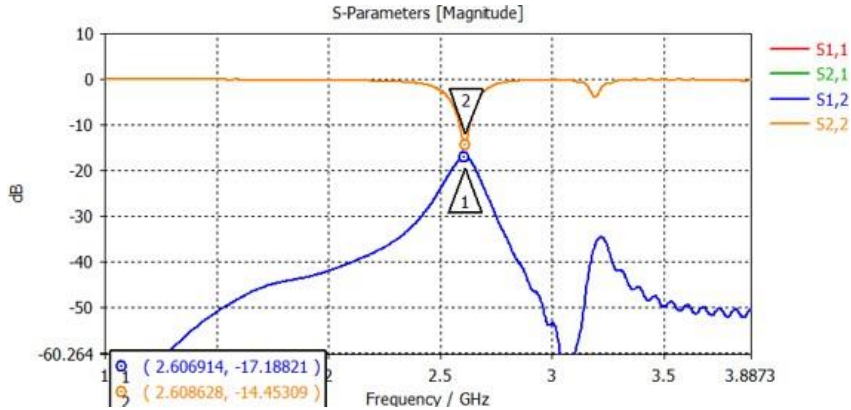

Figure 4.12: s11 and s21 parameters for the setup with the bone model placed centrally between the two antennas, highlighting the reflection and transmission characteristics of the system

With the bone placed at **150 mm**, distance from both antennas, s11 decreased to

48

-14.45 dB, indicating no change in reflection. While s21 dropped significantly to -17.18 dB, reduced transmission. These changes demonstrate how the bone model introduces additional losses and modifies signal behaviour at varying distances.

4.2 SAR Analysis

Specific Absorption Rate (SAR) is a measure of the rate at which the body absorbs electromagnetic energy when exposed to a radiofrequency (RF) electromagnetic field. It quantifies the power deposited per unit mass of tissue, typically expressed in watts per kilogram (W/kg). SAR is critical in ensuring the safety of RF devices, as excessive absorption of energy can cause tissue heating and potential harm. The SAR formula is given as:

$$\text{SAR} = \frac{\sigma E^2}{\rho},$$

Where, σ is the electrical conductivity of the tissue (in S/m), E is the electric field strength (in V/m), and ρ is the density of the tissue (in kg/m^3). In this equation, σ determines the rate at which the tissue conducts electrical current, E^2 represents the local intensity of the electric field, and ρ ensures normalization by the tissue's mass density.
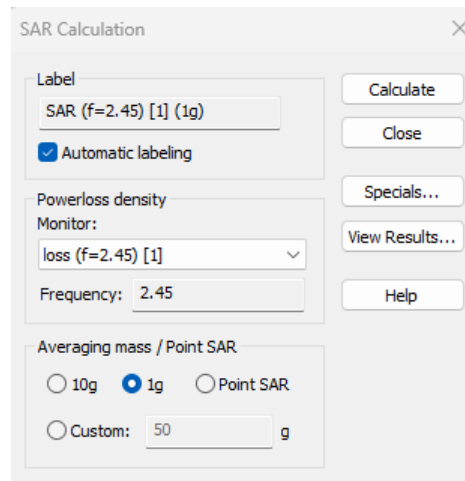
Figure 4.13: SAR calculation settings in CST Studio, showing the selection of the 1 g averaging mass for SAR analysis at a frequency of 2.45 GHz

For the current model, the values for σ (electric conductivity), ρ (density), and dielectric permittivity (ε) were explicitly defined. These values govern the propagation

49

of the electromagnetic wave within the modeled bone layers and directly influence the energy absorption and resultant SAR. In Figure 4.13 At 50 W power input and 2.45 GHz, the FCC regulatory standard for localized SAR is 1.6 W/kg, averaged over a 1 g volume of tissue [46]. This standard ensures safety by limiting the energy deposition to levels that do not induce harmful thermal effects.

The SAR averaging volume is a crucial aspect of the analysis. Regulatory bodies typically define SAR as an average over a specified mass of tissue, such as 1 g (FCC) or 10 g (ICNIRP). In CST, the averaging process calculates the absorbed power within the tissue volume corresponding to the chosen mass and normalizes it by the tissue density. For the given model, where the total mass is 3.5 g, a 1 g averaging volume was selected to align with FCC standards. From CST, SAR value of 0.294 W/kg, obtained from the 1 g analysis, as shown in fig4.14, is well below the FCC safety limit of 1.6 W/kg. The color map of SAR analysis highlights the localized energy absorption across the tissue model, with the highest absorption regions indicated by red. This value indicates that the energy absorbed by the tissue at a frequency of 2.45 GHz, even with an input power of 50 W, remains within safe exposure limits.
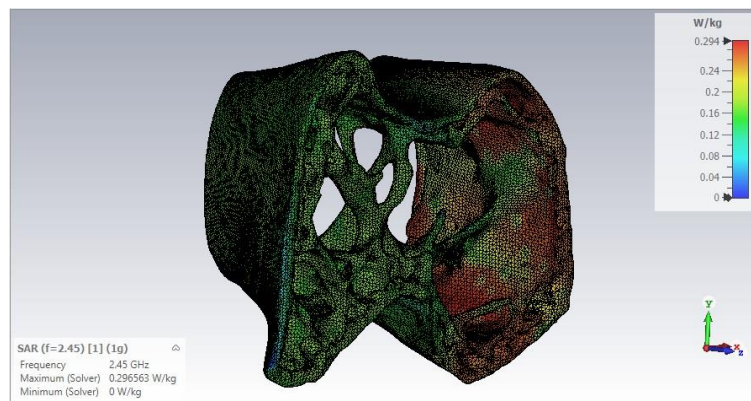
Figure 4.14: Visualization of SAR distribution for 1 g averaging mass at a frequency of 2.45 GHz, showing a maximum SAR value of 0.296 W/kg

The result confirms that the electromagnetic energy is distributed effectively within the model, ensuring compliance with regulatory standards. This approach ensures that the SAR computation is both localized and compliant with regulatory requirements.

One critique, however, lies in the simplification of tissue characteristics, as the model assumes constant values for conductivity, density, and permittivity, potentially overlooking the complex variability and heterogeneity in these properties across different

50

individuals or tissue types. Moreover, while the 1g averaging volume adheres to the FCC standard, the model does not account for potential variations in tissue composition or localized effects that may arise in other tissue volumes (e.g., 10g averaging, as per ICNIRP standards). A more comprehensive study, incorporating these factors, could yield more robust safety assurances for varied clinical scenarios. Nonetheless, the results from this SAR analysis affirm that, under the specified conditions, the RF-based system remains within safety limits for bone health evaluation.

4.3   Experimental Testing

For the experimental setup, two identical antennas were fabricated and positioned in a face-to-face configuration to evaluate their real time performance by using a vector network analyzer (VNA).

4.3.1   Autonomous Antenna Testing

Initially, the experiment was conducted without the bone model to assess the individual performance of each antenna. The primary focus was to measure the gain values of the fabricated standalone antenna in an anechoic chamber, at both the design frequency of 2.45 GHz and the observed operating frequency of 2.6 GHz. Measurements were performed in two distinct planes— the co-plane and the cross-plane— to thoroughly evaluate the antenna's radiation characteristics and performance across various orientations. Whereas, the co-plane and cross-plane measurements represent the polarization characteristics of the antenna's radiated field. The co-plane refers to the gain in the plane of the desired polarization of the antenna (typically the plane of maximum radiation). In contrast, the cross-plane refers to the gain in the orthogonal plane, representing the unwanted or undesired polarization component.

Whereas, the co-plane and cross-plane measurements represent the polarization characteristics of the antenna's radiated field. The co-plane refers to the gain in the plane of the desired polarization of the antenna (typically the plane of maximum radiation). In contrast, the cross-plane refers to the gain in the orthogonal plane, representing the unwanted or undesired polarization component.

Experimental testing at 2.45 GHz revealed that the gain in the co-plane was measured at 2.363 dB, while in the cross-plane, the gain was marginally higher at 2.923 dB. At 2.6 GHz, a significant increase in gain was observed in both planes, with the co-plane gain reaching 5.847 dB and the cross-plane gain at 4.787 dB. These findings, presented in Table 4.1, highlight a noticeable improvement in gain as the frequency increased from 2.45 GHz to 2.6 GHz. This enhancement in gain can be attributed to

potential variations in the antenna's resonant characteristics, influenced by the fabrication process or material properties, which may have altered the antenna's resonant frequency and radiation efficiency. Such frequency-dependent variations are typical in antenna behavior, where resonance and impedance matching are sensitive to subtle changes in the physical dimensions and dielectric properties of the antenna.

Table 4.1. Gain in dB of the Standalone Antenna at 2.45 GHz and 2.6 GHz Measured in Co-Plane and Cross-Plane

Frequency (GHz)	Gain (dB) Co-Plane	Gain (dB) Cross-Plane
2.45	2.363	2.923
2.6	5.847	4.787

When compared to the simulation setup, which predicted a gain of 3.051dB at 2.45 GHz, the experimental results show a slight discrepancy. The co-plane gain in the anechoic chamber was observed to be lower than the simulated value, while the cross-plane gain slightly exceeded the simulation. These differences can be attributed to various factors, including fabrication tolerances, connector losses, and the real-world imperfections that differ from idealized simulation conditions.

Overall, the experimental testing in the anechoic chamber provide valuable insight into the actual performance of the fabricated antenna. This shift in operating frequency to 2.6 GHz was also reflected in all the other parameters as well. The radiation patterns for the antenna were measured at 2.45 and 2.60 GHz for both the E-plane and H-plane configurations, as shown,

In Figure 4.15, the azimuthal plane exhibits a relatively uniform and omnidirectional radiation pattern. Maximum radiation occurs along certain directions, with minor variations and lobes in intensity. The amplitude shows consistency across most of the 360°range, indicative of a stable performance in this plane. Whereas, the elevation plane shows a less uniform pattern compared to the azimuthal plane. The amplitude of the radiation is lower in several regions compared to the azimuthal plane.

In Figure 4.16, the plots provide insights into the azimuthal (red curve) and elevation (blue curve) radiation characteristics in each orientation. The azimuthal plane exhibits a stable radiation pattern with the main lobe directed prominently along 0°. Radiation is relatively consistent across the surrounding angles, indicating good directivity along the desired axis. Elevation Radiation (Blue Curve), shows a more irregular distribution, with smaller lobes present in different directions. The E-plane demonstrates strong directivity, making it suitable for applications requiring a focused beam along a specific direction.

Patch Antenna ISM Band:2.45GHz (red:Elevation,blue:Azimuthal) Patch Antenna ISM Band:2.45GHz (red:Elevation,blue:Azimuthal)

(a) At 2.45 GHz, E-plane when the antenna is oriented in standard upright position

(b) At 2.45GHz, H-plane when the antenna is tilted at 90° position
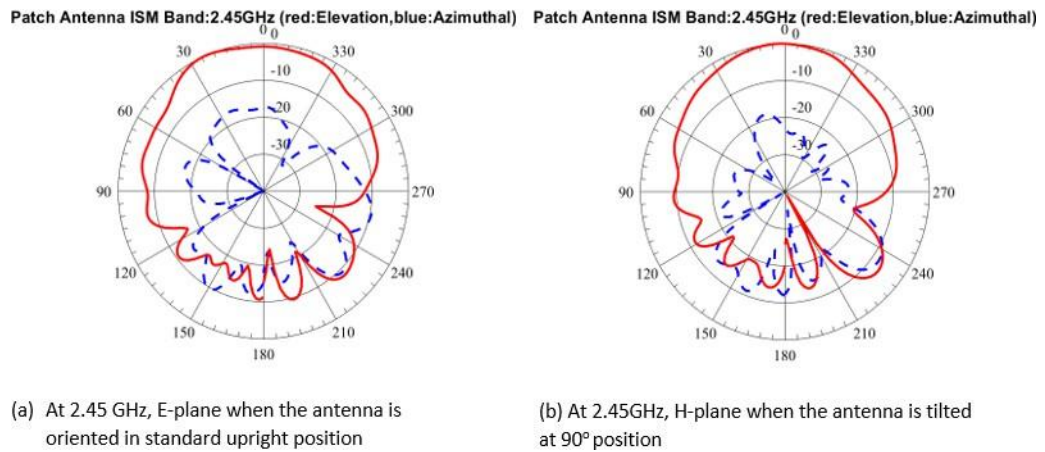
Figure 4.15: Measured Radiation pattern for (a) the patch antenna operating at 2.45 GHz in Plane 1 and (b) the patch antenna operating at 2.45 GHz in Plane 2, during experimental testing in the anechoic chamber, is plotted with azimuthal (blue) and elevation (red) planes.

Patch Antenna ISM Band:2.60GHz (red:Azimuthal,blue:Elevation) Patch Antenna ISM Band:2.60GHz (red:Azimuthal,blue:Elevation)

(a) At 2.60 GHz, E-plane when the antenna is oriented in standard upright position

(b) At 2.60 GHz, H-plane when the antenna is tilted at 90° position
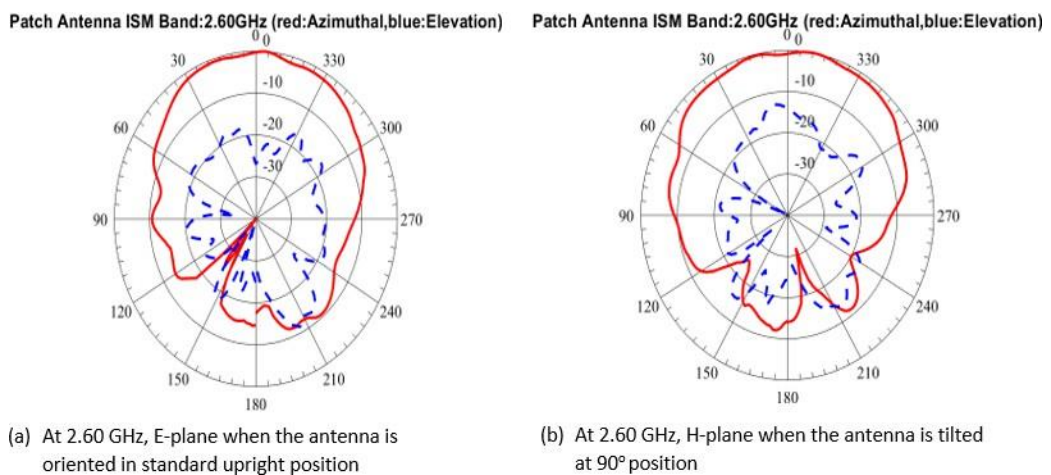
Figure 4.16: Measured Radiation pattern for (a) the patch antenna operating at 2.60 GHz in Plane 1 and (b) the patch antenna operating at 2.60 GHz in Plane 2, during experimental testing in the anechoic chamber, is plotted with azimuthal (red) and elevation (blue) planes.

The comparison of radiation patterns at 2.45 GHz and 2.60 GHz highlights notable variations due to the antenna's resonant frequency shift. At 2.45 GHz, the radiation pattern shows moderate stability but exhibits less directivity, with evident nulls and sidelobes, especially in the elevation plane. However, at 2.60 GHz, the radiation pat-

tern becomes more focused and directional in the azimuthal plane, with increased gain and reduced sidelobe levels.

Frequency shift from 2.45 GHz to 2.6 GHz after fabrication is a well-known occurrence in antenna design, typically resulting from variations in fabrication processes and material properties. This phenomenon has been extensively explored in several research studies. [47] discusses how deviations in geometry parameters from their nominal values can lead to frequency shifts, particularly in narrowband and multiband antennas. [48] analyzes the impact of material and fabrication tolerances on antenna performance, highlighting the challenges in maintaining desired resonant frequencies due to manufacturing variations. [49] examines how manufacturing tolerances affect the resonance frequency, emphasizing the need for precise fabrication to achieve intended performance.

The measured s11 parameter for one antenna was observed to be -15.54 dB at a resonance frequency of 2.63 GHz, while the s22 parameter for the second antenna was recorded as -21.99 dB at 2.61 GHz as shown in Figure 4.17. These values were obtained from experimental data processed and plotted using MATLAB. Ideally, both parameters s11 and s22 should exhibit identical values, but discrepancies arose due to minor variations introduced during the fabrication process. Such variations are attributed to slight imperfections in the material properties, manufacturing tolerances, or assembly alignment, which are challenging to control precisely. These findings provide an essential comparison point against the simulated parameters to validate the design's real-world performance.
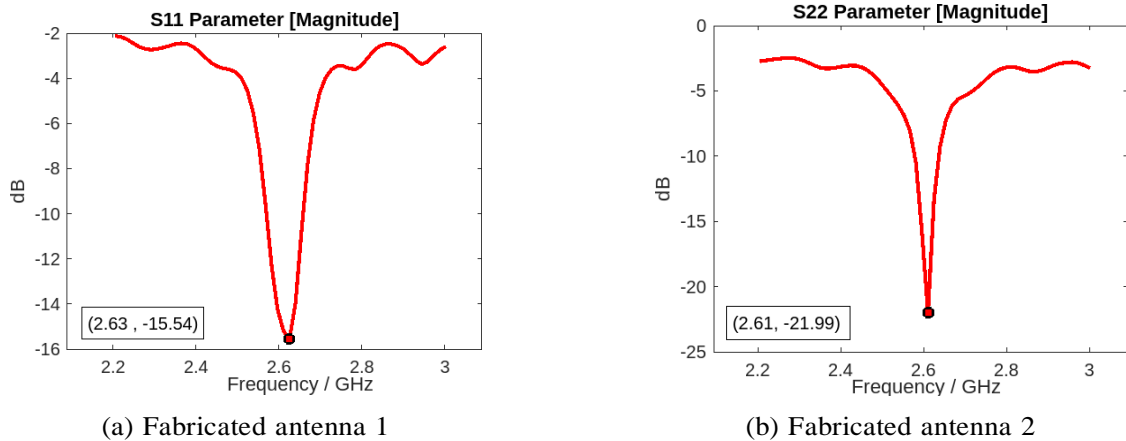

(a) Fabricated antenna 1   (b) Fabricated antenna 2

Figure 4.17: S-parameters of the fabricated antennas where, (a) s11 of -15.54dB at 2.63GHz, (b) s22 of -21.99dB at 2.61GHz

The other parameter that was visualized with the help of s-parameters was the Voltage Standing Wave Ratio (VSWR) of the fabricated antennas was analyzed through MATLAB-generated graphs. The measured VSWR value was 1.40 at 2.63Ghz as shown in Figure 4.18. This demonstrates acceptable matching at the operating frequencies, further confirming the operational efficiency of the fabricated antennas. However, if we
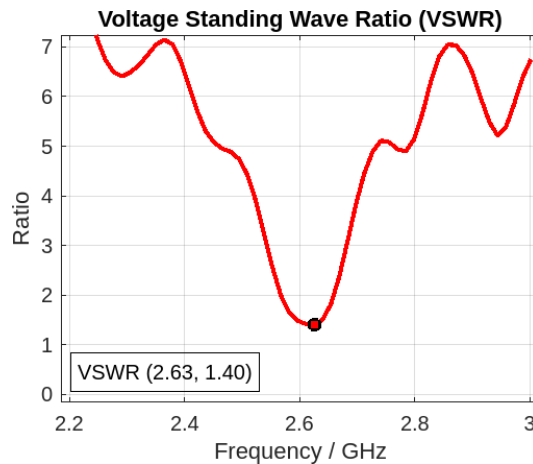
Figure 4.18: VSWR of fabricated antenna 1.40 at 2.63GHz

draw a comparison of the simulated VSWR value of 1.196 at 2.45GHz with the measured value of 1.40 at 2.63GHz. The observed deviation can primarily be attributed to a shift in both frequency and magnitude. While the simulation model was set to operate at 2.45 GHz, the fabricated antennas exhibited a new operational frequency at 2.6 GHz. This discrepancy is a result of inherent limitations in the fabrication process, including material inconsistencies, alignment errors, and the absence of idealized conditions found in the simulation model. Additionally, environmental factors such as connector losses and variations in the experimental setup further contribute to these discrepancies. Despite these deviations, the measured Voltage Standing Wave Ratio (VSWR) remains within acceptable limits, indicating minimal reflection and ensuring efficient power transmission within the system. These detailed observations provide crucial insights for understanding the antenna's performance and will be instrumental in validating the system's robustness under real-world conditions.

4.3.2   Antenna Testing with Bone Model

In this subsection, the experimental results obtained from testing the fabricated antenna setup using a Vector Network Analyzer (VNA) are presented. The experiment was conducted with two face-to-face antennas, with a cork material placed equidistant between them, simulating a bone model. The cork was chosen as a proxy for bone tissue due to its comparable dielectric properties, allowing for an approximation of the

electromagnetic interactions between the antennas and bone.

Cork is often used as a surrogate material in experiments simulating bone due to its similar dielectric properties with bone. While it is not an exact replica of bone tissue, cork's structure and composition allow it to mimic certain key characteristics, such as its relative permittivity (dielectric constant) and attenuation behavior.

Cork has a relatively low dielectric constant, somewhat similar to that of bone, particularly in the frequency range used for many RF-based measurements. This makes it suitable for studying electromagnetic interactions and wave propagation in a controlled, replicable way. Additionally, cork has a porous structure that can mimic bone's cellular pattern, influencing how electromagnetic waves interact with it. While bones exhibit varying densities in their cortical and trabecular regions, cork offers a material with low density and a comparable structural pattern.

Moreover, cork is a readily available, non-toxic material, making it practical for use in experiments where cost and safety are considerations. Although not identical to bone, cork's electromagnetic wave attenuation and absorption characteristics provide a reasonable approximation of how waves might propagate through bone tissue, particularly in low-frequency RF studies. In this way, cork therefore serves as an appropriate surrogate for bone in initial studies and proof-of-concept experiments, offering an effective approximation for bone-like behavior in terms of electromagnetic wave interactions.

As shown in Figure 4.19 measurements were taken for three different separation distances between the antennas: 100 mm, 200 mm, and 300 mm, the same as in the software simulations so we can easily compare the software results with the experimental results. The primary focus of this analysis was on the S parameters, specifically
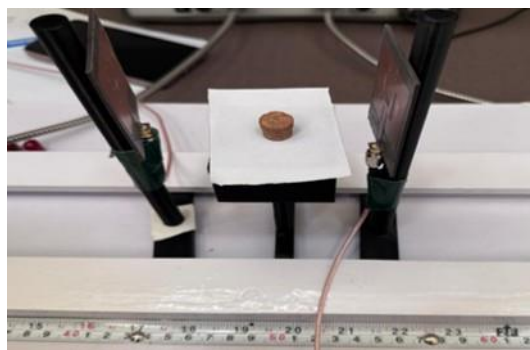

Figure 4.19: Experimental setup showing the placement of two fabricated antennas, with a 100 mm separation distance. A cork material in center, representing a bone model

s11 (reflection coefficient) and s21 (transmission coefficient), to evaluate the interaction of the electromagnetic waves with the cork model in the experimental setup. Results provided a comprehensive understanding of the impact of varying distances on signal attenuation and energy absorption by the porous bone model. We have already discussed the results of the parameters s11 and s22 for fabricated antennas without the cork (bone model), the next measured value as in Figure 4.20, was when we placed the cork at a distance of 50mm from the antennas and an overall distance of 100mm between the antennas. In the presented graph, s11 paramters are represented with a
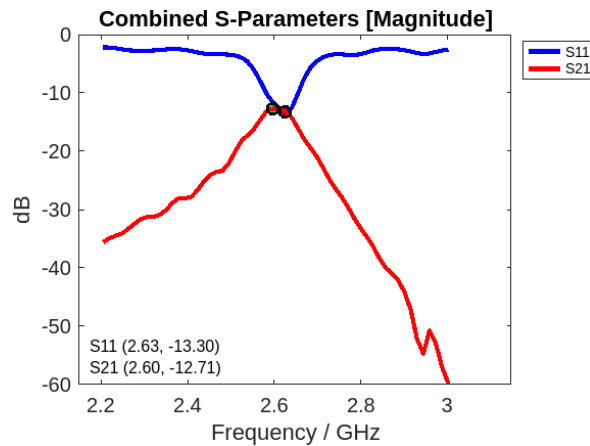
Figure 4.20: s11 and s21 parameters for the setup with the bone model placed centrally between the two antennas, highlighting the reflection and transmission characteristics of the system

blue line, and marker indicates the value of -13.30 dB at 2.63 GHz frequency. This finding is significant for bone health applications, as it suggests that electromagnetic wave transmission through bone-like materials can be efficiently achieved, minimizing reflection losses that could impact the accuracy of diagnostic or therapeutic applications.

Whereas, s21 paramters are represented with a red line and the marker indicates its value of -12.71dB at 2.60 GHz. The s11 parameter exhibits good impedance matching at this frequency, indicating that minimal energy is reflected back to the antenna, ensuring efficient coupling at the operating frequency of 2.6GHz for fabricated antennas. The s21 parameter, on the other hand, reflected the amount of energy transmitted through the cork material. This value indicates moderate signal attenuation, as about 6.3% of the input power was transmitted through the system, with the remaining energy either absorbed or lost due to the interaction with the cork model and the propagation path. An ideal system with minimal signal loss should have an s21 closer to -10 dB or better.

Figure 4.21: In experimental setup, cork model positioned at the center, 100 mm from each antenna, with a total separation of 200 mm between Antenna 1 and Antenna 2

To demonstrate the next experiment of varying distance, in Figure 4.21 (cork) bone model was placed at a distance of 100mm from both antennas, creating a total distance of 200mm between the antennas.

Reflecting on the impact of S21, specially for applications in bone health, this attenuation is crucial, as it directly correlates with the tissue's electromagnetic properties, which can be used to assess bone density and structure. Bone mineral density, a key factor in bone health, influences how electromagnetic waves are absorbed or transmitted, as denser bone tissues typically lead to greater signal attenuation. The observed moderate signal loss in this experiment provides insights into how bone health could affect RF signal propagation, where diseased or osteoporotic bone may show even higher attenuation, offering potential for early diagnosis through electromagnetic wave-based techniques.

After simulation, it was evident that the increase in distance caused significant deviations in the s-parameters. At a distance of 100mm bewtween both the antennas, s11 was measured at -13 dB, and s21 was -12 dB at 2.63 and 2.60 GHz respectively. With the cork model in center and antennas at 200 mm distance from eachother as shown in Figure 4.22, s11 decreased to -14.56 dB, and s21 reduced to -17.36 dB at 2.63GHz. This trend indicates a slight frequency shift in s21, improved impedance matching for s11 parameter, meaning the antenna is coupling more energy into the system instead of reflecting it back. For our experiment as the distance increases, the transmitted signal has to travel through a larger portion of the medium (air and cork). The cork material, representing a lossy porous bone, may absorb more energy, which could lead to less reflection(s11) and higher values of transmission loss(s21 further decreases).
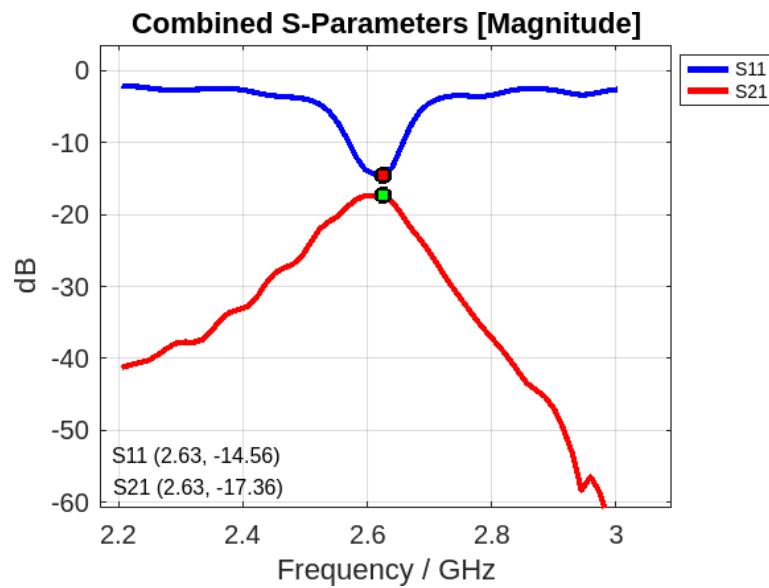
Figure 4.22: s11 and s21 parameters for the overall distance of 200mm

Lastly, the distance was set at a total distance of 300mm and 150mm at each side from the cork, as shown in Figure 4.23. As a result for this last configuration, graph
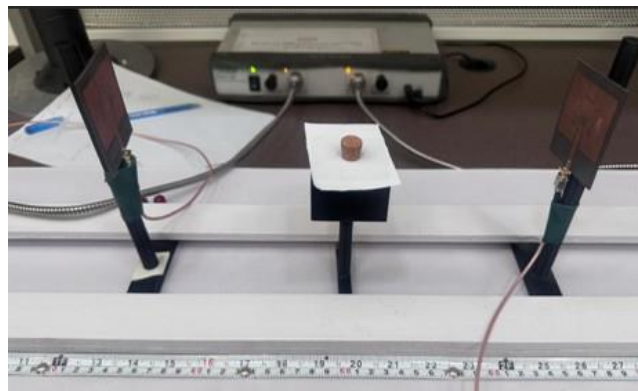
Figure 4.23: In experimental setup, cork model positioned at the center, 150 mm from each antenna, with a total separation of 300 mm between Antenna 1 and Antenna 2

in Figure 4.24 highlights the effect of distance on the measurement by placing the cork model at a distance of 150mm. At a frequency of 2.63 GHz s11 has a value -15.54dB. While, a slight frequency shift towards left has been observed in s21, it has a vakue of -21.01dB at 2.61GHz. The distance has a direct effect on the values of transmission coefficient (s21), as the distance increases signal attenuation further increases, causing

59

a drop in the values of s21.

At shorter distances, such as 100 mm, the s21 values are relatively higher because the path loss and material absorption are minimal. However, as the distance increases to 200 mm and 300 mm, the s21 values decrease, reflecting the increased losses in transmission. This relationship highlights the combined effects of propagation losses and material properties, with the porous nature of the cork model playing a significant role in attenuating the signal as it passes through.
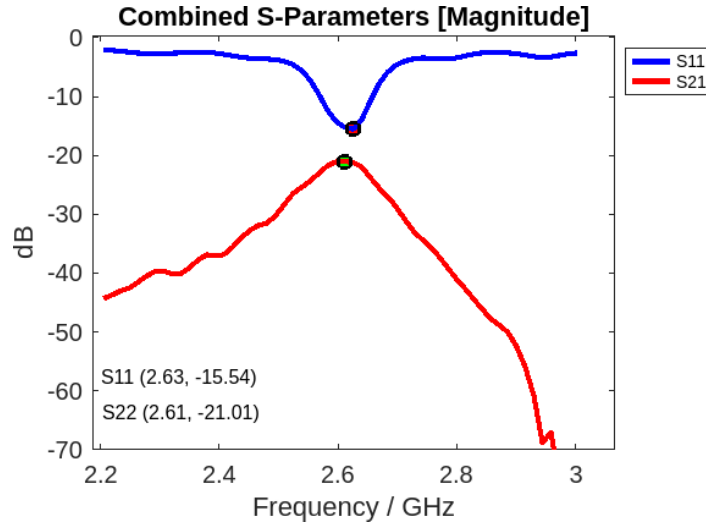
Figure 4.24: s11 and s21 parameters for the experimental setup at a total distance of 300mm

4.4   Correlation of Experimental Testing and Simulation

The comparison between CST software simulations using segmented 3D bone model and experimental measurements for the fabricated antenna setup, with a bone model represented by a cork, reveals several critical insights into the differences and similarities in system behavior. Initially, the microstrip patch antenna design in software simulations was targeted to operate at the standard frequency of 2.45 GHz, which corresponds to the ISM band. However, after fabrication and experimental testing, the operating frequency shifted to approximately 2.60 GHz. This shift can be attributed to several factors. During fabrication, minor deviations in material properties (e.g., the available dielectric constant of the substrate) and dimensional tolerances (e.g., slight

variations in antenna dimensions) can cause changes in the antenna's resonant behavior. Additionally, environmental factors, such as imperfections in the soldering process or coupling effects in the experimental setup, could further contribute to this frequency shift. This highlights the inherent differences between idealized software simulations and real-world physical implementations.

When the antennas were placed in a face-to-face configuration during testing, the s11 (input reflection coefficient) and s22 (output reflection coefficient) responses were observed to be similar in both software simulations and experimental measurements. Both simulations and experiments showed these parameters to resonate around the shifted operating frequency of 2.60 GHz. Software simulations typically provide ideal results due to the absence of physical imperfections or environmental interferences. In simulations, the response of s11 and s22 was symmetric, and the transmission coefficients s21(forward transmission) and s12 (reverse transmission) also showed identical behavior due to the idealized conditions. However, during experimental testing of the fabricated antennas, slight variations were observed between these parameters, especially in s21 and s12 These variations can be attributed to real-world effects such as material losses, fabrication tolerances, and minor asymmetries in the experimental setup.

In software simulations, s11 exhibited a deep resonance dip, reflecting excellent impedance matching and minimal reflection at the operating frequency. Similarly, s21 showed higher transmission values, indicating minimal attenuation as shown in a combined graph in Figure 4.25. In comparison, the measured experimental results showed a
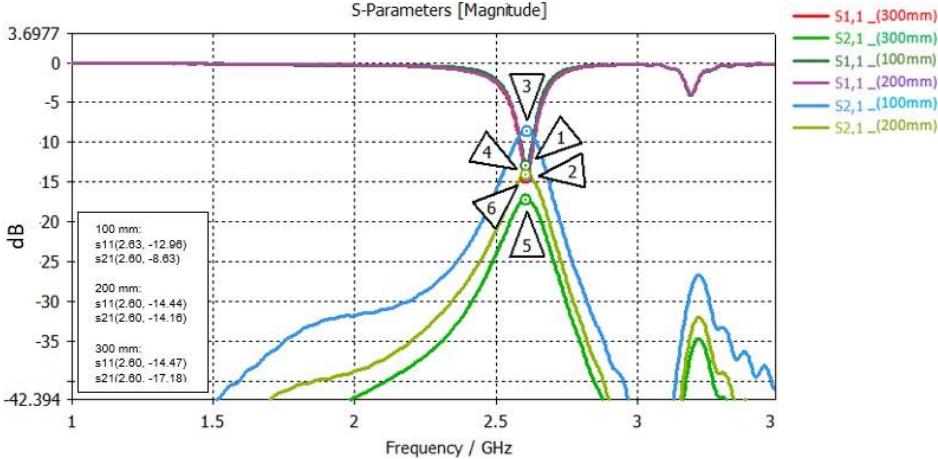
Figure 4.25: Simulated magnitude plot of s11 and s21 for antenna distances of 100 mm, 200 mm, and 300 mm. Markers indicate key resonance points

similar trend for s11 but with a slightly less pronounced dip, likely due to real-world imperfections and additional reflection at the antenna interfaces. For s21, the experi-
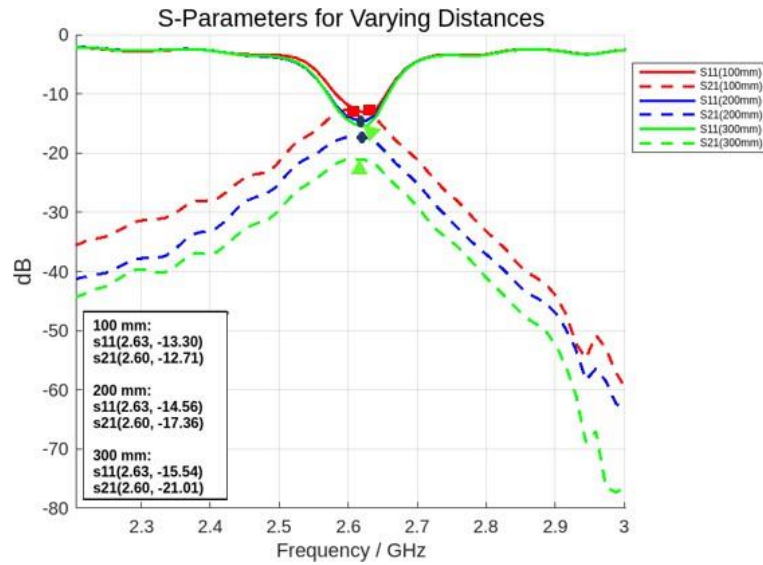
Figure 4.26: s11 (solid lines) and s21 (dashed lines) for varying antenna distances (100 mm, 200 mm, 300 mm), with markers indicating minimum s11 and maximum s21 values near 2.60 GHz

mental results showed lower transmission values compared to simulations, highlighting the influence of material absorption and dielectric losses introduced by the cork model and other setup components.

A combined graph for experimental values is as shown in Figure 4.26. The comparison underscores that while software simulations provide an idealized prediction of antenna behavior, experimental measurements reveal the impact of real-world imperfections and environmental factors. Despite these differences, the trends observed in both approaches align, offering valuable insights in bone health evaluation, as an application of wearable antennas.

Chapter 5

CONCLUSIONS

This research successfully developed a non-invasive RF-based prototype for assessing bone health, addressing critical limitations in traditional diagnostic techniques such as DEXA scans. The primary goal was to create an innovative solution that leverages radio frequency (RF) technology, offering a safer, more accessible, and cost-effective alternative. Through the integration of detailed 3D modeling, microstrip patch antenna design, and experimental validation, the study demonstrated the feasibility of using RF technology for bone health assessment. The findings of this research not only show the potential for RF-based solutions in monitoring bone density and composition but also pave the way for future advancements in non-invasive diagnostics for conditions like osteoporosis and osteopenia.

A novel approach was introduced to perform analysis on an anatomically realistic bone model, comprising two distinct bone layers: cortical and trabecular. This approach differs significantly from existing literature, where simplified human phantoms or bovine bones are often used, with porosity artificially introduced by drilling. By constructing a detailed 3D model from high-resolution CT scans and assigning accurate dielectric properties to each bone layer, this study achieved a more precise representation of bone anatomy. This allowed for more realistic evaluations of electromagnetic wave interactions with bone structures, offering new insights into how RF signals respond to bone porosity and dielectric variations.

The design and optimization of two identical microstrip patch antennas operating at 2.45 GHz within the ISM band formed the core of this study. These antennas were tailored for on-body applications and demonstrated their ability to analyze electromagnetic energy transfer. Through simulations and experimental setups, variations in s11 (reflection) and s21 (transmission) parameters were observed. These trends highlighted the influence of dielectric properties and antenna positioning on signal behavior, providing critical insights into bone porosity and structure.

The integration of simulation and experimental validation reinforced the reliability of this approach. Despite challenges such as frequency shifts in fabricated antennas and the use of cork as a bone model, the overall correspondence between simulation predictions and experimental results supported the viability of this RF-based methodology. Furthermore, the study demonstrated how distance and dielectric properties influenced antenna performance, providing a robust foundation for understanding these parameters in biological contexts.

This research represents a significant advancement in orthopedic diagnostics, with implications for the development of portable and wearable diagnostic tools. Such devices could enable early intervention for bone health issues, particularly in regions where conventional diagnostic technologies are unavailable or impractical. While the limitations and recommendations for future work are discussed in next chapter, this study establishes a strong basis for further exploration of RF-based medical diagnostics.

In conclusion, this research highlights the transformative potential of RF technology in bone health assessment. By introducing a non-invasive, anatomically realistic alternative, this study contributes to the broader efforts to improve skeletal health diagnostics and enhance global healthcare. The findings underscore the promise of RF-based methods in addressing critical gaps in bone health management, early detection of diseases like osteopenia and real-world applications.

Chapter 6

LIMITATIONS AND FUTURE RECOMMENDATION

The current study, while effectively demonstrating the interaction of electromagnetic waves with a bone model using custom-designed antennas, reveals several limitations that must be addressed to realize its full potential for practical applications. One notable limitation is the use of cork material as a bone substitute. While cork serves as an initial prototype, it does not accurately replicate the complex dielectric and structural properties of human or bird bones.

Future work should focus on utilizing physical testing of actual bird bones to more closely emulate the physical characteristics of bone tissue. This adjustment will refine the accuracy of wave propagation studies, providing a more reliable foundation for future diagnostic applications in bone health.

Another area for enhancement is the antenna design. Although the fabricated antenna operates efficiently within the ISM band at 2.60 GHz, exploring alternative antenna shapes and targeting different frequencies within the ISM band could optimize the system for various medical applications. These modifications could further improve the system's precision and adaptability, ensuring its relevance across a broader range of clinical contexts.

Additionally, reducing the frequency shift between simulations and experimental results through improvements in antenna fabrication would enhance the alignment between theoretical models and real-world performance, making the technology more reliable.

Moreover, integrating a substrate with a higher dielectric constant than the currently used Rogers 5880 substrate would allow for a smaller antenna design, facilitating a more compact and portable system without compromising performance.

The current prototype remains a lab-scale configuration, presenting a key challenge for its practical application. A critical next step involves miniaturizing the system into a wearable device, such as a wristwatch, which would make bone density measurement more accessible and user-friendly. This wearable device could seamlessly integrate with existing medical technologies, offering a non-invasive alternative to current bone health diagnostics like DEXA scans. However, the transition from prototype to practical tool requires comprehensive validation through clinical trials and collaboration with healthcare professionals. This collaboration will be vital for refining the device's accuracy and usability, ensuring that it meets the clinical standards required for routine medical applications.

Moreover, the study highlights a limitation in performance as the distance between antennas increases, particularly concerning signal attenuation in the s21 values. This suggests that the current system may face challenges in patients with larger anatomical dimensions or in cases requiring measurements over greater distances. Future work should focus on optimizing the antenna design and transmission system to mitigate these losses, expanding the potential applicability of the device. Additionally, environmental factors such as external interference and surrounding dielectric materials were not fully considered in this study, yet these variables could substantially impact real-world performance. Future studies should incorporate more complex experimental environments to account for such factors.

In conclusion, while the present study lays a robust foundation for a novel approach to bone health evaluation, substantial room exists for enhancement. Key advancements include refining the prototype design, employing anatomically realistic bone models, integrating high-dielectric substrates to reduce antenna size, collaborating with medical experts, and addressing practical limitations to enable the system's translation into a viable medical device. These efforts will not only enhance the reliability and accuracy of the RF-based bone health assessment system but will also pioneer new possibilities for the integration of RF technology into healthcare diagnostics, positioning it as a valuable tool in the future of non-invasive medical imaging and bone health monitoring.

REFERENCES

[1] N. L. Kazanskiy, S. N. Khonina, and M. A. Butt, "A review on flexible wearables – recent developments in non-invasive continuous health monitoring," *Sensors and Actuators A: Physical*, vol. 366, p. 114993, 2024. [Online]. Available: https://www.sciencedirect.com/science/article/pii/S0924424723008427

[2] S. R. Kerketta and D. Ghosh, "Microwave sensing for human bone health evaluation," *AEU-International Journal of Electronics and Communications*, vol. 127, p. 153469, 2020.

[3] J. D. Barros, J. J. de Oliveira, and S. G. da Silva, "Characterization of bone tissue using microstrip antennas," in *2010 Annual International Conference of the IEEE Engineering in Medicine and Biology*. IEEE, 2010, pp. 3982–3985.

[4] T. Zhou, P. M. Meaney, M. J. Pallone, S. Geimer, and K. D. Paulsen, "Microwave tomographic imaging for osteoporosis screening: a pilot clinical study," in *2010 Annual International Conference of the IEEE Engineering in Medicine and Biology*. IEEE, 2010, pp. 1218–1221.

[5] M. Ahmad, L. Yang, and R. Anjum, "Implementation of the convolutional perfectly matched layer (cpml) in the face-centered cubic (fcc) fdtd method," *Waves in Random and Complex Media*, pp. 1–12, 2022.

[6] A. Nouri Moqadam and R. Kazemi, "Design of a novel dual-polarized microwave sensor for human bone fracture detection using reactive impedance surfaces," *Scientific Reports*, vol. 13, no. 1, p. 10776, 2023.

[7] W. Zeinelabedeen and R. Uyguroglu, "A study on health care monitoring of femoral shaft fracture healing by using implanted antenna for wireless in-to-out body channel communication," *Journal of Electromagnetic Waves and Applications*, vol. 36, no. 5, pp. 722–742, 2022.

[8] D. Lee, J. Velander, T. Blokhuis, K. Kim, and R. Augustine, "Preliminary study on monitoring the progression of osteoporosis using uwb radar technique in distal femur model," *Electronics Letters*, vol. 52, no. 8, pp. 589–590, 2016.

[9] A. Singh, D. Mitra, B. Mandal, P. Basuchowdhuri, and R. Augustine, "A review of electromagnetic sensing for healthcare applications," *AEU - International Journal of Electronics and Communications*, vol. 171, p. 154873, 2023. [Online]. Available: https://www.sciencedirect.com/science/article/pii/S1434841123003473

[10] A. Mohan and N. Kumar, "Implantable antennas for biomedical applications: a systematic review," *BioMedical Engineering OnLine*, vol. 23, no. 1, p. 87, 2024. [Online]. Available: https://doi.org/10.1186/s12938-024-01277-1

[11] International Diabetes Federation, *IDF Diabetes Atlas*, 10th ed. Brussels, Belgium: International Diabetes Federation, 2021, available at: https://www.diabetesatlas.org. [Online]. Available: https://www.diabetesatlas.org

[12] T. Karacolak, A. Z. Hood, and E. Topsakal, "Design of a dual-band implantable antenna and development of skin mimicking gels for continuous glucose monitoring," *IEEE Transactions on Microwave Theory and Techniques*, vol. 56, no. 4, pp. 1001–1008, 2008.

[13] S. Afroz *et al.*, "Implantable sic based rf antenna biosensor for continuous glucose monitoring," in *SENSORS, 2013 IEEE.* IEEE, 2013.

[14] X. Liu, Z. Wu, Y. Fan, and M. Tentzeris, "A miniaturized csrr loaded wide-beamwidth circularly polarized implantable antenna for subcutaneous real-time glucose monitoring," *IEEE Antennas and Wireless Propagation Letters*, vol. 16, pp. 1–1, 01 2016.

[15] L. Song and Y. Rahmat-Samii, "An end-to-end implanted brain–machine interface antenna system performance characterizations and development," *IEEE Transactions on Antennas and Propagation*, vol. 65, no. 7, pp. 3399–3408, 2017.

[16] P. Zakavi, N. C. Karmakar, and I. Griggs, "Wireless orthopedic pin for bone healing and growth: Antenna development," *IEEE transactions on antennas and propagation*, vol. 58, no. 12, pp. 4069–4074, 2010.

[17] S. Symeonidis, W. G. Whittow, M. Zecca, and C. Panagamuwa, "Bone fracture monitoring using implanted antennas in the radius, tibia and phalange heterogeneous bone phantoms," *Biomedical Physics & Engineering Express*, vol. 4, no. 4, p. 045006, 2018.

[18] S. B A, R. K, N. Padala, J. Bandi, and A. D. T, "A miniaturized implantable antenna for health care monitoring," in *2024 Asia Pacific Conference on Innovation in Technology (APCIT)*, 2024, pp. 1–4.

[19] Y. Liu, Q. Zhang, and L. Wang, "A circularly polarized implantable antenna for bone condition monitoring in microsystems," *IEEE Transactions on Antennas and Propagation*, vol. 69, no. 12, pp. 4567–4575, 2021.

[20] S. Aslam, Y. Tan, and A. Chauraya, "A folded dipole rfid tag antenna for continuous bone health monitoring," in *2017 IEEE International Conference on RFID Technology and Applications (RFID-TA)*, 2017, pp. 1–6.

[21] R. Koul and A. Bharadwaj, "Ultra-wideband (uwb) antennas for wireless bone health monitoring: Neural monitoring and bone density analysis," *IEEE Sensors Journal*, vol. 21, no. 14, pp. 15 632–15 640, 2021.

[22] Y. Wang, R. Chen, and L. Zhang, "Evaluation of an rf wearable device for non-invasive real-time hydration monitoring," in *2017 IEEE Body Sensor Networks (BSN)*, 2017, pp. 1–4.

[23] Z. Feng, L. Ma, and Q. He, "Bone health assessment using photoacoustic temporal profile analysis," *Ultrasound in Medicine and Biology*, vol. 47, no. 8, pp. 2102–2115, 2021.

[24] M. Fatemi and A. Alizad, "Acoustic rf signals for monitoring bone healing: Sensitivity to structural variations," *Journal of the Acoustical Society of America*, vol. 145, no. 5, pp. 3083–3094, 2019.

[25] A. Kwan, J. Fung, and J. Ng, "Non-invasive detection of osteoporotic bone loss using photothermal radiometry and modulated luminescence," in *Proceedings of SPIE - The International Society for Optical Engineering*, vol. 6841, 2008, p. 68410D.

[26] A. Aziz, D. Ahmad, T. A. Shila, S. Rana, R. R. Hasan, and M. A. Rahman, "On-body circular patch antenna for breast cancer detection," in *2019 IEEE international electromagnetics and antenna conference (IEMANTENNA)*. IEEE, 2019, pp. 029–034.

[27] A. R. Chishti, A. Aziz, K. Aljaloud, F. A. Tahir, Q. H. Abbasi, Z. U. Khan, and R. Hussain, "A sub 1 ghz ultra miniaturized folded dipole patch antenna for biomedical applications," *Scientific Reports*, vol. 13, no. 1, p. 9900, 2023.

[28] S. N. Makarov, G. M. Noetscher, S. Arum, R. Rabiner, and A. Nazarian, "Concept of a radiofrequency device for osteopenia/osteoporosis screening," *Scientific Reports*, vol. 10, no. 1, p. 3540, 2020.

[29] N. Shrivastava, D. Ghosh, and P. K. Sahu, "A clustering approach for understanding bone health using rf transmission characteristics," *IEEE*

Antennas and Propagation Workshops and Conferences, 2024. [Online]. Available: https://typeset.io/papers/a-clustering-approach-for-understanding-bone-health-using-rf-56bb5cwv3pq1

[30] S. N. Makarov, W. Appleyard, P. D. Carberry, H. V. Tankaria, G. M. Noetscher, and A. Nazarian, "Novel on-body microwave antenna array testbed for highly-sensitive measurements of wrist bone signature," in *Proceedings of the International Symposium on Antennas and Propagation*, 2017. [Online]. Available: https://typeset.io/papers/novel-on-body-microwave-antenna-array-testbed-for-highly-3ohxpbyhti

[31] S. E. Sarma, R. Bhattacharyya, J. E. Siegel, S. N. R. Kantareddy, U. A. Armengol, and P. Sen, "System and method for wireless sensing of health monitoring," Patent, 2020. [Online]. Available: https://typeset.io/papers/system-and-method-for-wireless-sensing-of-health-monitoring-5a91ekltm9

[32] Z. Liu, Y.-P. Hsu, and M. M. Hella, "An rf powering system with adaptive impedance matching for individual health monitoring applications," in *Proceedings of the International Conference of the IEEE Engineering in Medicine and Biology Society*, 2016. [Online]. Available: https://typeset.io/papers/an-rf-powering-system-with-adaptive-impedance-matching-for-1uojcd9yyj

[33] A. Bhattacharya and Others, "Dual-band microstrip antennas for biomedical applications," *IEEE Transactions on Antennas and Propagation*, 2021.

[34] P. Joshi and Others, "Compact patch antennas for bone health monitoring," *Journal of Electromagnetic Waves and Applications*, 2020.

[35] V. Patel and Others, "Enhanced on-body antenna performance using ebg structures," *IEEE Sensors Journal*, 2021.

[36] R. Singh and S. Verma, "Dielectric substrate effects on biomedical antenna performance," *Microwave and Optical Technology Letters*, 2022.

[37] R. Jain and Others, "Microstrip antennas for dielectric property analysis in bones," *International Journal of RF and Microwave Computer-Aided Engineering*, 2023.

[38] T. Wiczenbach, L. Pachocki, K. Daszkiewicz, P. Łuczkiewicz, and W. Witkowski, "Development and validation of lumbar spine finite element model," *PeerJ*, vol. 11, p. e15805, 2023.

[39] G. Albuquerque, A. Cruz, D. Carvalho *et al.*, "A method based on non-ionizing microwave radiation for ancillary diagnosis of osteoporosis: a pilot study," *BioMed Eng OnLine*, vol. 21, p. 70, 2022. [Online]. Available: https://doi.org/10.1186/s12938-022-01038-y

[40] B. D. M. Pinheiro, A. L. P. D. S. Campos, D. D. A. de Carvalho, A. S. Cruz, R. A. de Medeiros Valentim, N. V. R. Veras, and J. P. Q. dos Santos, "The influence of antenna gain and beamwidth used in osseus in the screening process for osteoporosis," *Scientific Reports*, vol. 11, no. 1, p. 19148, Sep 2021.

[41] U. Ali, S. Ullah, B. Kamal, L. Matekovits, and A. Altaf, "Design, analysis and applications of wearable antennas: A review," *IEEE Access*, vol. 11, pp. 14 458–14 486, 2023.

[42] M. Shakhawat Hossen, M. Tariqul Islam, A. Hoque, A. M. Alenezi, P. Kirawanich, M. Hafiz Baharuddin, Y. S. Faouri, and M. Arafatur Rahman, "Revolutionizing osteoporosis and bone fracture diagnostics: The emergence of microwave antenna technology," *IEEE Access*, vol. 12, pp. 160 418–160 440, 2024.

[43] G. K. Soni, D. Yadav, A. Kumar, and M. V. Yadav, "Design of dual-element mimo antenna for wearable wban applications," in *2023 IEEE Microwaves, Antennas, and Propagation Conference (MAPCON)*, 2023, pp. 1–5.

[44] S. Alhuwaidi and T. Rashid, "A novel compact wearable microstrip patch antenna for medical applications," in *2020 International Conference on Communications, Signal Processing, and their Applications (ICCSPA)*, 2021, pp. 1–6.

[45] Z. C. Fei, N. Ramli, P. L. Jethi, T. Khalifa Sanossi, and N. H. Abd Rahman, "Performance analysis of rectangular microstrip patch antenna with different substrate material at 2.4 ghz for wlan applications," in *2021 7th International Conference on Space Science and Communication (IconSpace)*, 2021, pp. 46–49.

[46] R. E. Fields, "Evaluating compliance with fcc guidelines for human exposure to radiofrequency electromagnetic fields," *Oet Bull*, vol. 65, no. 10, pp. 1–57, 1997.

[47] C. Oikonomopoulos-Zachos and M. Martínez-Vázquez, "Effect of technological tolerances in the design of a 60 ghz ltcc antenna," in *2010 IEEE Antennas and Propagation Society International Symposium*, 2010, pp. 1–4.

[48] S. Koziel and A. Pietrenko-Dabrowska, "Tolerance optimization of antenna structures by means of response feature surrogates," *IEEE Transactions on Antennas and Propagation*, vol. 70, no. 11, pp. 10 988–10 997, 2022.

[49] D. J. Bem and R. J. Katulski, "An analysis of the influence of the manufacturing accuracy on the microstrip antenna properties," in *Ninth International Wrocław Symposium on Electromagnetic Compatibility*, 1988, pp. 261–264.